Distinguishing between physical and biological controls on the spatial variability of pCO_2: a novel approach using OMP water mass analysis (St. Lawrence, Canada)

Ashley Dinauer[1] and Alfonso Mucci

GEOTOP and Department of Earth and Planetary Sciences, McGill University, 3450 University Street, Montreal, QC H3A 0E8, Canada

[1] Corresponding author (ashley.dinauer@mail.mcgill.ca)

Published in Marine Chemistry:

DINAUER A. and MUCCI A. (2018) Distinguishing between physical and biological controls on the spatial variability of pCO_2: a novel approach using OMP water mass analysis (St. Lawrence, Canada). Marine Chemistry **204:**107-120. https://doi.org/10.1016/j.marchem.2018.03.007.

Abstract. Present-day air-sea CO_2 flux estimates in the coastal ocean are subject to large uncertainties due to its heterogeneous nature and concomitant lack of data. Factors controlling the dissolved inorganic carbon (DIC) and CO_2 fluxes vary within and between coastal subsystems, hampering the development of robust upscaling and modeling techniques. By applying a multi-tracer, quantitative water mass analysis, physical and biogeochemical factors can be differentiated. This study adopts an expanded version of optimum multiparameter (OMP) water mass analysis, an inverse modeling technique, to estimate the mixing fractions of predefined source water masses as well as the contribution of biological activity (photosynthesis, respiration) at a given observation point in the surface mixed layer that exchanges CO_2 gas with the atmosphere. We apply the method to hydrographic, nutrient, and inorganic carbon data collected in the Estuary and Gulf of St. Lawrence, the world's largest estuarine system and an excellent analogue of the more general coastal environment. Biological activity is identified as the dominant control on mixed-layer CO_2 partial pressure (pCO_2) dynamics along the St. Lawrence land—ocean continuum, explaining the upstream to downstream shift from pCO_2 supersaturation (net heterotrophy) to pCO_2 undersaturation (net autotrophy). Although mixing of freshwater and seawater along the Estuary is the major contributor to the DIC pool, it contributes little (or negligibly) to the spatial variability of surface-water pCO_2.

Keywords. Carbon cycle; Coastal ocean; Estuaries; Water mass analysis; OMP analysis; Water mass tracers; St. Lawrence Estuary; Gulf of St. Lawrence; Laurentian Channel

1 Introduction

The ocean has absorbed ca. 30% of the total anthropogenic carbon dioxide (CO_2) emitted to the atmosphere from fossil fuel burning and land-use changes since the beginning of the industrial era (Doney et al., 2009), yet accurate quantification of organic and inorganic carbon cycling and fluxes in the coastal ocean — where land, ocean and atmosphere interact — remains challenging. The very large uncertainty associated with present-day air-sea CO_2 flux estimates in coastal waters, including rivers, estuaries, tidal wetlands, and the continental shelf, impedes meaningful predictions of the effects of climate change on future fluxes (Bauer et al., 2013). The coastal ocean occupies only ~7% of the global ocean surface area, but it plays a major role in biogeochemical cycles because it (1) receives massive inputs of terrestrial organic matter and nutrients through continental runoff and groundwater discharge; (2) exchanges matter and energy with the open ocean; and (3) is one of the most geochemically and biologically active areas of the biosphere, accounting for significant

fractions of marine primary production (~14 to 30%), organic matter burial (~80%), sedimentary mineralization (~90%), and calcium carbonate deposition (~50%) (Gattuso et al., 1998).

Although the carbon cycle of the coastal ocean is acknowledged to be a major component of the global carbon cycle and budget, it is poorly quantified (Bauer et al., 2013). Constraining the exchanges and fates of different forms of carbon along the land—ocean continuum is so far incomplete, owing to limited data coverage and large physical and biogeochemical variability within and between coastal subsystems (e.g., hydrological and geomorphological differences, differences in the magnitude and stoichiometry of organic matter inputs). Changes in freshwater discharge, coupled with higher-frequency (e.g., diurnal and seasonal) and higher-magnitude (e.g., large excursions of salinity and temperature) natural variability compared to the open ocean, further hamper our current understanding of the factors controlling the fluxes and cycling of organic and inorganic carbon in the coastal ocean (Fassbender et al., 2016). The concentration and speciation of dissolved inorganic carbon (DIC) determine the direction and magnitude of air-sea exchanges of CO_2, with the former being influenced by complex interactions between a number of physical and biogeochemical processes. In the surface mixed layer, the effects of transport processes (circulation, mixing), biological activity (photosynthesis, respiration), and gas exchange are particularly important.

To differentiate between the physical and biogeochemical drivers affecting DIC fluxes in the coastal ocean, one must estimate the relative contributions of freshwater and seawater to the observed mixture as well as quantitatively assess the influence of important biogeochemical processes. Optimum multiparameter (OMP) water mass analysis, an inverse modeling technique, is a standard tool in oceanography for the quantitative description of water mass structures. It utilizes the observed fields of hydrographic properties (e.g., temperature, salinity, dissolved oxygen, and nutrients) to resolve the distributions of different water masses in a given region of mixing. An expansion of the method to include Redfield stoichiometry corrects for the non-conservative behavior of dissolved oxygen and nutrients resulting from organic matter remineralization (Karstensen and Tomczak, 1998). Although OMP analysis has been successfully applied at both regional and oceanic scales, it does not usually apply to the sunlit surface mixed layer, where water mass properties are non-conservative and display high seasonal variations due to air-sea interaction and CO_2 uptake by photosynthetic organisms (Poole and Tomczak, 1999).

This paper presents a further extension of the OMP analysis method and its application to the surface mixed layer. By incorporating the apparent oxygen utilization

(AOU) to determine the sign convention (+/–) for the Redfield ratios, i.e., whether the stoichiometric ratios reflect net respiration or net photosynthesis, our method accounts for the effects of organic matter remineralization and phytoplankton photosynthesis in the observed tracer fields. In this study, we apply the improved method to hydrographic, nutrient, and inorganic carbon data collected in the Estuary and Gulf of St. Lawrence, the world's largest estuarine system and an excellent analogue of the more general coastal environment. The aim of the analysis is to determine the physically- and biologically-induced changes of DIC and the extent to which they control surface-water CO_2 partial pressure (pCO_2) dynamics along the St. Lawrence land—ocean continuum. Multi-tracer, quantitative water mass analysis, as it is shown here, provides a valuable technique for improved mechanistic descriptions of inorganic carbon cycling processes in the coastal ocean — a task of increasing importance for the development of proper upscaling strategies and for achieving closure on the oceanic and global carbon budgets.

2 Data and methods

2.1 Site description—St. Lawrence Estuary and Gulf

The Estuary and Gulf of St. Lawrence, at the southern limit of the subarctic region in eastern Canada, connects the waters of the Great Lakes, the second largest terrestrial freshwater reservoir in the world, with those of the northwest Atlantic Ocean. Because of its large physical dimensions and unimpeded connection to continental shelf and slope waters, the St. Lawrence Estuary (SLE) is fairly unique in that its character is more oceanic than most estuaries. Beginning at the upstream limit of salt water intrusion near Île d'Orléans (~5 km downstream of Québec City), the SLE stretches 400 km seaward to Pointe-des-Monts where it widens into the Gulf of St. Lawrence (GSL) (El-Sabh and Silverberg, 1990), a marginal sea with an area of 250,000 km^2 whose principal connection to the open shelf is through Cabot Strait (Coote and Yeats, 1979). The largest source of freshwater to the SLE is the St. Lawrence River, the second largest river system in North America. Mean annual discharge of the St. Lawrence River near Québec City is ~10,000 $m^3\ s^{-1}$, amounting to about 80% of the total freshwater input to the Estuary (Ingram and El-Sabh, 1990), whereas the freshwater runoff from the Saguenay Fjord and Manicouagan River on the north shore contributes about 10–13% and 9–10%, respectively (Tee, 1990).

Traditionally, the SLE is divided into two segments based on bathymetry and hydrographic features. The Upper St. Lawrence Estuary (USLE) is relatively narrow (2 to 24 km) and mostly shallow (<30 m) with an uneven, fairly complex bottom

topography. Although it displays a strong lateral salinity gradient, its water column ranges from well-mixed to partially stratified. In contrast, the Lower St. Lawrence Estuary (LSLE) is wider (30 to 50 km) and deeper (~300 m) and displays a smoother, less variable bottom topography. The dominant bathymetric feature of the LSLE is the Laurentian Channel (or Trough), a deep, central, U-shaped glaciated valley that extends 1,240 km from the eastern Canadian continental shelf break through the GSL and into the LSLE (d'Anglejan, 1990). In summertime, the SLE can be described as a three-layer system on the basis of its thermal stratification (Gratton et al., 1988), with (1) a warm and relatively fresh surface layer (0–30 m) flowing out from the St. Lawrence River and Saguenay Fjord (Dufour and Ouellet, 2007), (2) a cold (~0 °C) and salty (S_P = 32 to 33) intermediate layer (30–150 m) formed by advection of the wintertime surface mixed layer from the GSL (Galbraith, 2006), and (3) a warmer (2 to 6 °C) and saltier (S_P = 33 to 35) deep layer (>150 m), of mixed Atlantic and Labrador shelf waters, flowing sluggishly from Cabot Strait into the Lower Estuary (Saucier et al., 2003; Gilbert et al., 2005). A detailed description of the physical oceanography of the St. Lawrence Estuary is given by Saucier and Chassé (2000) and Simons et al. (2010).

2.2 Sampling and sample analysis

The hydrographic data used in this study were collected during ten cruises aboard the R/V *Coriolis II* in the late spring or early summer between 2003 and 2016. Water sampling was conducted mainly along the central axis of the St. Lawrence Estuary and the Laurentian Channel. The sampling locations are shown in Fig. 1. Water samples were taken from discrete depths throughout the water column with 12 12L Niskin bottles mounted on a rosette sampler fitted with a SeaBird SBE 911 conductivity-temperature-depth (CTD) probe as well as a SBE-43 oxygen probe. Although the probes were calibrated by the manufacturer during the winter months preceding the cruises, discrete samples were taken from the Niskin bottles for laboratory measurements of practical salinity (S_P; Guildline Autosal 8400 salinometer calibrated with IAPSO standard seawater) and dissolved oxygen (DO; Winkler titration as described by Grasshoff et al., 1999) and the CTD records re-calibrated post-cruise. In addition, field and laboratory measurements were made of the following physical—chemical properties: pH_{NBS} and/or pH_T, total alkalinity (TAlk), soluble reactive phosphate (SRP), nitrate (NO_3), dissolved silicate (DSi), and the stable oxygen isotopic composition of water ($\delta^{18}O_{water}$).

Water samples for isotopic analysis were taken up into 13mL screw-top plastic test tubes. Samples were analyzed for the stable oxygen isotope ratio $^{18}O/^{16}O$ using the CO_2 equilibration method (Epstein and Mayeda, 1953) on a Micromass AquaPrep system and the CO_2 analyzed on a Micromass IsoPrime universal triple collector isotope ratio mass spectrometer in dual inlet mode at the Université du Québec à Montréal (Light

Stable Isotope Geochemistry Laboratory). Data were normalized against two internal reference waters, both calibrated against V-SMOW and V-SLAP. The oxygen isotope measurements are reported on the δ-scale in ‰ relative to Vienna Standard Mean Ocean Water (V-SMOW): $\delta^{18}O = (({}^{18}O/{}^{16}O)_{sample} / ({}^{18}O/{}^{16}O)_{VSMOW} - 1) \times 1000$. Based on replicate analyses of the samples, the average relative standard deviation of the measurements was better than 0.05‰.

Water samples were also analyzed for pH, TAlk, SRP, NO_3, and DSi. A detailed description of the analytical methods is found in Dinauer and Mucci (2017). For the purpose of applying a quantitative water mass analysis to the dataset, *in situ* temperature was converted to potential temperature and all concentrations were reported in the same units (i.e., μmol kg^{-1}). The potential temperature (θ) along with *in situ* density (ρ) and pressure (p) were calculated using the Gibbs Seawater (GSW) Oceanographic Toolbox (MATLAB-version 3.05; McDougall and Barker, 2011) of the Thermodynamic Equation of Seawater – 2010 (TEOS-10). The ρ values (kg m^{-3}) were used in the conversion of units.

2.3 Calculation of mixed-layer pCO_2 and temperature normalization

The CO_2 partial pressure (pCO_2) in seawater is a function of temperature, dissolved inorganic carbon, total alkalinity, and salinity. Because direct pCO_2 measurements were not available from the R/V *Coriolis II* cruises, pCO_2 values (μatm), as well as DIC concentrations (μmol kg^{-1}), were calculated from the measured pH (total or NBS scale) and TAlk (μmol kg^{-1}), at *in situ* temperature (°C), salinity (S_P), and pressure (dbar), using the CO2SYS program (MATLAB-version 1.1; van Heuven et al., 2011) and the carbonic acid dissociation constants (K_1, K_2) of Cai and Wang (1998) for estuarine waters. Whenever data were available, the contributions of phosphate and silicate to the TAlk were included in the calculations, but their contributions were negligible compared to the carbonate and borate alkalinities, particularly in surface waters. Based on the measurement accuracies of pH (±0.003) and TAlk (0.5%), we assign an overall uncertainty of ±9.7 μatm to the calculated pCO_2 using the error propagation routine of Orr et al. (2017).

The present work focuses on the inorganic carbon chemistry of the surface mixed layer (SML) that exchanges gases, heat, and water with the overlying atmosphere. To obtain a single value of surface-water pCO_2 at each sampling location, the pCO_2 data points in the SML were averaged. The mixed-layer depth (MLD) was defined using a density-based criterion ($\Delta\rho$ = 0.03 kg m^{-3}) (de Boyer Montégut et al., 2004). Given the low-resolution sampling above the thermocline, the mixed-layer dataset at each station was most often limited to a single data point (from ~2 or ~3m depth), although, in a

few cases, it included a sample collected at ~10m depth. In the following sections, surface-water pCO_2 will be taken to mean the SML-averaged pCO_2.

Among the state variables that determine pCO_2, the effects of temperature and DIC are the most important ones in surface seawater (Takahashi et al., 1993). The effect of temperature on pCO_2 is primarily the manifestation of changes in the equilibrium of the carbonate system in water. To remove this effect from the CO_2 signal, the pCO_2 data were normalized to the mean sea surface temperature of the study area ($pCO_2(\overline{SST})$, $\overline{SST}$ = 7.01 °C), using the temperature normalization method of Jiang et al. (2008). The net temperature dependence of pCO_2 was estimated as follows:

$$\Delta pCO_2(temp) = pCO_2(obs) - pCO_2\left(\overline{SST}\right) \quad (1)$$

where ΔpCO_2(temp) is the thermally-induced pCO_2 change due to temperature deviation from $\overline{SST}$, pCO_2(obs) is the *in situ* pCO_2, and $pCO_2(\overline{SST})$ is the temperature-normalized pCO_2. After correcting the CO_2 signal for temperature, spatial changes in surface-water $pCO_2(\overline{SST})$ can be attributed to the combined effects of physical and biological processes directly linked to the addition or removal of inorganic carbon in the surface mixed layer.

2.4 Inorganic carbon budget

The combined effects of water mass mixing, biological activity, and air-sea gas exchange on the observed DIC concentrations are summarized in the following budget:

$$DIC_{obs} = DIC_{mix} + \Delta DIC_{bio} + \Delta DIC_{gas} \quad (2)$$

where DIC_{obs} is the DIC observation, DIC_{mix} is the DIC contribution from mixing processes, ΔDIC_{bio} is the DIC change due to photosynthesis/respiration, and ΔDIC_{gas} is the DIC change due to gas exchange. The DIC_{mix} and ΔDIC_{bio} terms in the DIC budget can be derived directly from the model output of quantitative water mass analysis, as described in Section 2.5.2, whereas an accurate quantification of ΔDIC_{gas} proves more difficult due to the different time scales over which these processes operate. The net transfer of CO_2 gas across the air-sea interface occurs whenever its partial pressure in the mixed layer differs from that in the atmosphere. However, on short time scales (weeks to months), mixing and biological processes are likely to have a more significant effect on the mixed-layer DIC budget, given the relatively slow air-sea CO_2 gas exchange rate (generally on the order of several months to ~1 year; see Sabine and Key, 1998;

Sabine and Feely, 2007). Here, we quantify the effect of gas exchange on the DIC budget by subtracting DIC_{mix} and ΔDIC_{bio} from DIC_{obs}:

$$\Delta DIC_{gas} = DIC_{obs} - DIC_{mix} - \Delta DIC_{bio} \quad (3)$$

Positive values of ΔDIC_{gas} indicate DIC addition (CO_2 uptake), whereas negative values indicate DIC removal (CO_2 release). For comparison, ΔDIC_{gas} was also calculated from the air-sea flux of CO_2 gas:

$$\Delta DIC_{gas} = \frac{-F_{gas} \cdot t_{residence}}{MLD} \quad (4)$$

where F_{gas} is the air-sea CO_2 gas flux (mmol C m^{-2} d^{-1}) at a given observation point, $t_{residence}$ is the mean residence time of surface waters in the St. Lawrence Estuary (~4 months; Silverberg and Sundby, 1990), and MLD is the mean mixed-layer depth in the St. Lawrence system (assumed to be 20 m, intermediate between the MLD of the well-mixed Upper Estuary and that of the Gulf during spring; Saucier et al., 2003). The air-sea CO_2 flux calculation is described by Dinauer and Mucci (2017). Briefly, F_{gas} was calculated from the CO_2 gas transfer velocity, k, the solubility of CO_2 at *in situ* temperature and salinity (Weiss, 1974), K_0, and the difference between the partial pressures of CO_2 in the water, $pCO_2(water)$, and the air, $pCO_2(air)$, respectively, i.e.:

$$F_{gas} = k \cdot K_0 \cdot \left(pCO_2(water) - pCO_2(air)\right) \quad (5)$$

The difference between $pCO_2(water)$ and $pCO_2(air)$ determines the direction of gas exchange across the air-sea interface. Positive values of F_{gas} indicate CO_2 release (local CO_2 source), whereas negative values indicate CO_2 uptake (local CO_2 sink).

2.5 Quantitative water mass analysis

In this study, we used a further development of the optimum multiparameter (OMP) analysis method to distinguish between the effects of water mass mixing (DIC_{mix}) and biological activity (ΔDIC_{bio}) at a given observation point. In so doing, we also differentiate between the physically- and biologically-induced changes of $pCO_2(\overline{SST})$. The number and spatial coverage of water mass tracers (i.e., temperature, salinity, $\delta^{18}O_{water}$, dissolved oxygen, nutrients, DIC, and TAlk) available from observations represented the most important limitations on the application of OMP analysis. We

restrict our spatial analysis to the observational data collected during the R/V *Coriolis II* cruise of May 2016. These data are available at sufficient resolution, including the availability of data in the water mass formation regions, to allow for a detailed analysis of the DIC budget along the St. Lawrence land—ocean continuum.

2.5.1 Optimum multiparameter (OMP) analysis

OMP analysis, as introduced by Tomczak (1981) and extended by Tomczak and Large (1989), optimizes the information contained in a hydrographic dataset by fitting a set of water mass tracers to a linear inverse mixing model. The model is used to determine the relative contributions (or mixing fractions) of various water masses that best reproduce the observations within the dataset. Classical OMP analysis assumes that all tracers are conservative, restricting its application to small oceanic regions (i.e., over horizontal distances on the order of hundreds of kilometers) where biogeochemical effects can be reasonably ignored. In its classical form, OMP analysis treats the mixing fractions as the only unknown variables, although there is no reason, in principle, why the model cannot include other variables. Oceanic scale applications of OMP analysis became possible through a general extension of the method to account for the effects of organic matter remineralization on dissolved oxygen and nutrient concentrations (Karstensen and Tomczak, 1998). The non-conservative behavior of oxygen and nutrients is accounted for by introducing Redfield ratios and an additional variable (representing the remineralized phosphate concentration) into the model. This is equivalent to the use of preformed nutrient concentrations, but, as an added advantage, the amount of biogeochemical changes can be derived directly from the model output (Tomczak, 1999).

In reality, the biogeochemical processes affecting dissolved oxygen and nutrient concentrations typically vary because of net phytoplankton photosynthesis in the euphotic zone and net microbial respiration of organic matter below it. Even in its extended form, OMP analysis does not usually apply to the sunlit surface mixed layer, where both temperature and salinity, in addition to the biogeochemical (non-conservative) tracers, undergo changes unrelated to mixing. Furthermore, the extended OMP analysis model accounts only for the biogeochemical changes due to organic matter remineralization, and although recent modeling efforts have accounted for the effects of denitrification and calcium carbonate dissolution (Hupe and Karstensen, 2000; Schneider et al., 2005), photosynthesis is not considered to be an important contributor to the biogeochemical tracer distributions. This assumption does not hold in the present study, which focuses on the important contributors to the DIC budget in the surface mixed layer.

To account for both remineralization and photosynthesis, the OMP analysis method is further expanded to include the concept of apparent oxygen utilization (AOU). The AOU represents the amount of oxygen utilized in the oxidation of organic matter since a water parcel was last in contact with the atmosphere or residing in the surface mixed layer. Assuming that the surface water is in equilibrium with the overlying atmosphere (100% saturated), AOU (μmol kg^{-1}) is given by:

$$AOU = DO^* - DO \quad (6)$$

where DO is the observed oxygen concentration and DO^* is the saturation oxygen concentration, a function of temperature and salinity (Benson and Krause, 1984). For simplicity, we neglect the effect of bubble injection and the differential gas exchange rate across the air-sea interface on the saturation oxygen concentration (Ito et al., 2004). In our study area, surface waters are supersaturated by an average of 15% and undersaturated by 6%, and, in the absence of inert gas measurements, we assume that this departure from equilibrium is solely the result of biological activity. This simplifying assumption allows us to expand the biogeochemical part of the OMP analysis model, using AOU as a means of predicting the biogeochemical regime and thus the sign (±) of the Redfield stoichiometric ratios at a given observation point. In other words, when AOU >0, we assume that microbial respiration exceeds phytoplankton photosynthesis (net respiration), i.e., nutrients and DIC are released while oxygen is consumed ($C/N/P/-O_2$). Alternatively, when AOU <0, we allow photosynthetic activity to compose the observational data, whereby nutrients and DIC are taken up and oxygen is released (net photosynthesis; $-C/-N/-P/O_2$). This procedure is justified provided that biologically-induced changes are rapid compared to other processes occurring at the sea surface (e.g., gas exchange).

Note that, as well as being subject to change through mixing and biological activity, the DIC concentrations of a water parcel are affected by air-sea gas exchange at the surface and by the formation/dissolution of calcium carbonate in the water column. The latter process is negligible in the study area, given that the Estuary's phytoplankton community is dominated by diatoms and dinoflagellates (Devine et al., 2015) and pelagic carbonate-secreting organisms (coccolithophores, pteropods) are found only at very low concentrations in the Gulf and in the Strait of Belle Isle (Levasseur et al., 1994; Cantin et al., 1996; Levasseur et al., 1997). The effect of air-sea gas exchange on both the DIC and DO observations represents a source of error inherent to the application of OMP analysis in the surface mixed layer, where fluxes of heat, salt, and dissolved gases continuously occur.

2.5.2 Model equations

We used a set of equations that is formally similar to the linear system used by Schneider et al. (2005) but predicts different biogeochemical changes (i.e., changes due to remineralization and photosynthesis):

$$
\begin{aligned}
&f_1 T_1 + \cdots + f_n T_n + 0 = T_{obs} + R_T \\
&f_1 S_1 + \cdots + f_n S_n + 0 = S_{obs} + R_S \\
&f_1 \delta^{18}O_1 + \cdots + f_n \delta^{18}O_n + 0 = \delta^{18}O_{obs} + R_{\delta^{18}O} \\
&f_1 DO_1 + \cdots + f_n DO_n \pm r_{O_2/P} \Delta P = DO_{obs} + R_{DO} \\
&f_1 SRP_1 + \cdots + f_n SRP_n \pm r_{P/P} \Delta P = SRP_{obs} + R_{SRP} \\
&\qquad (7) \\
&f_1 NO_{3,1} + \cdots + f_n NO_{3,n} \pm r_{N/P} \Delta P = NO_{3,obs} + R_{NO_3} \\
&f_1 DSi_1 + \cdots + f_n DSi_n \pm r_{Si/P} \Delta P = DSi_{obs} + R_{DSi} \\
&f_1 DIC_1 + \cdots + f_n DIC_n \pm r_{C/P} \Delta P = DIC_{obs} + R_{DIC} \\
&f_1 TAlk_1 + \cdots + f_n TAlk_n \pm r_{N/P} \Delta P = TAlk_{obs} + R_{TAlk} \\
&f_1 + \cdots + f_n + 0 = 1 + R_\Sigma
\end{aligned}
$$

On the left-hand side of the equations, f are the mixing fractions of n different predefined source water masses that compose each observed tracer field through conservative mixing (e.g., f_1S_1 + … + f_nS_n). In the biogeochemical part of the model, the change in phosphate due to biological activity (ΔP) is linked via the Redfield ratios ($\pm r_{tracer/P}$) to predict the changes in the remaining biogeochemical tracers (ΔO_2, ΔN, ΔSi, ΔC). The ΔC is equivalent to the ΔDIC_{bio} in equation (2), whereas the ΔO_2 is equivalent to the AOU only in the biogeochemical sense. Because their calculation is different, some of the problems associated with the reliable estimation of AOU (e.g., supersaturated surface waters and the nonlinear dependence of the oxygen solubility on temperature; Broecker and Peng, 1982; Hupe and Karstensen, 2000) are avoided in the model representation of ΔO_2. The right-hand side of the equations is given by the observational data and their respective residuals (R). The last row expresses the condition of mass conservation, which is an additional mixing constraint. The resulting system of equations is overdetermined (more equations than unknowns), allowing a non-negative least squares (NNLS) technique to find the solution to the unknowns (f_n, ΔP).

As detailed by Tomczak and Large (1989), the equations are normalized and weighted to ensure parameters of incommensurable units are comparable and to account for environmental variability and measurement inaccuracies. Weights were calculated using the equation of Tomczak and Large (1989):

$$W_j = \sigma_j^2 \,/\, \delta_{j,max} \quad (8)$$

where σ_j is the standard deviation of parameter j over the entire dataset (a measure of the ability of parameter j to resolve differences in water mass content), and $\delta_{j,max}$ is the largest of the water mass variances for parameter j. Under the weighting scheme, the weight allocated to each parameter reflects its range-to-precision ratio, making the mass conservation residuals an objective indicator of the quality of the solution. A low mass conservation residual indicates that the properties of the water sample are well represented by the source water masses considered. Because a NNLS technique is used and several sources of error exist (e.g., source water mass definition errors, measurement errors), the residuals will never be zero (Hupe and Karstensen, 2000). An upper limit of 5% was applied to identify and remove data points poorly described by the model (Poole and Tomczak, 1999).

2.5.3 Redfield ratios

As introduced by Redfield et al. (1963), Redfield ratios relate the changes in dissolved oxygen, nutrient, and inorganic carbon concentrations in a water parcel due to microbial oxidation of particulate organic matter:

$$(C_{106}H_{263}O_{110}N_{16}P) + 138\,O_2 \rightarrow 106\,CO_2 + 16\,HNO_3 + H_3PO_4 + 122\,H_2O \quad (9)$$

According to this formula, the stoichiometric ratio of ΔC to ΔO_2 (i.e., the respiratory quotient, RQ) is ~0.77, although investigations by Anderson and Sarmiento (1994) and Hedges et al. (2002) have shown that RQ may vary significantly (0.57 to 0.80).

In our application, we used the "classical" C:–O_2 Redfield ratio of 106/–138, whereas we estimated the nitrate and silicate Redfield ratios for the study area. Silicate is, in contrast to nitrate and phosphate, regenerated via chemical dissolution of biogenic silica tests (shells) rather than by microbial oxidation of organic soft tissue. Because silica is found only in marine organisms with siliceous skeletons (e.g., diatoms), stoichiometric ratios relating ΔSi to ΔP are subject to significant regional variations and must be estimated for the region under consideration (Poole and Tomczak, 1999). In this study, the N:P and Si:P ratios were determined by linear regression of nutrient data extracted from below the surface layer (depth >30 m) as shown in Fig. 2. The N:P ratio from this analysis was 12/1 (R^2 = 0.79, standard error of 0.42), whereas the Si:P ratio was 23/1 (R^2 = 0.76, standard error of 0.71). The N:P ratio derived for the study area is somewhat lower than the 16/1 ratio given by Redfield et al. (1963), but lower N:P ratios in coastal and estuarine environments are not unusual (Coote and Yeats, 1979).

2.5.4 Selection and definition of source water masses

The first step in the OMP analysis process is to define the major water masses that contribute to the water column structure of the study area. In the framework of OMP analysis, a source water mass is a body of water with a common formation history, having its origin in a particular formation (source) region (Tomczak, 1999). For biogeochemical studies, it is critical that these source water masses be defined either in the outcrop regions or where the water mass enters the basin of interest (Schneider et al., 2005). Defining the source water masses "upstream" of the investigated region allows for the assumption that the observed tracer fields "downstream" result from mixing between water masses originating from the formation regions and, over long distances, biogeochemical cycling activity (Hupe and Karstensen, 2000). The actual parameter values for the source water masses can be found in the literature or, preferably, in reference to observations in the water mass formation regions.

As discussed earlier, the general circulation pattern of the water masses in the St. Lawrence is estuarine with net seaward flow in the surface layer and landward flow in the intermediate and deep layers. The literature suggests that up to four major water masses contribute to the three-layer vertical structure found in the summer months. Warm and relatively fresh surface waters from the St. Lawrence River (SLR) and the Saguenay Fjord and rivers on the north shore of the Lower Estuary (SFNS) contribute to the surface layer (Dufour and Ouellet, 2007), whereas the intermediate and deep layers are dominated by cold (~0 °C) and salty (S_P = 32 to 33) intermediate water formed by advection of the wintertime surface mixed layer from the GSL, often referred to as the Gulf summertime cold intermediate layer or CIL (Galbraith, 2006), and warmer (2 to 6 °C) and saltier (S_P = 33 to 35) deep water formed by advection of mixed Atlantic and Labrador shelf waters that enter the GSL through Cabot Strait (Saucier et al., 2003; Gilbert et al., 2005) (hereinafter referred to as Labrador/Atlantic deep water or LADW).

In the present application of OMP analysis, the source water mass definitions were derived from hydrographic data within the formation regions relevant to this study, i.e., the water mass formation regions for SLR, SFNS, LADW, and CIL. Fig. 3 shows the hydrographic stations used to represent each formation region. Defining the boundaries of these regions required a compromise between (1) minimizing the influence of other water masses and of biological processes on the water mass definitions and (2) encompassing the full range of environmental variability (across space and time) of water mass properties in the formation regions (Poole and Tomczak, 1999). Because of their similar catchment geology and stable oxygen isotopic signatures (P. del Giorgio, UQAM, pers. comm., 2017), the Saguenay River and the major north-

shore rivers (e.g., the Manicouagan, Moisie, Romaine, Outardes and Betsiamites rivers) were grouped as one source water mass. The water mass formation regions for LADW and CIL were identified by a salinity maximum at >150m depth and a temperature minimum in the depth range 30–150 m, respectively.

Data extracted from each formation region were combined and averaged to give the definition values and standard deviations for temperature, salinity, $\delta^{18}O_{water}$, dissolved oxygen, nutrients, DIC, and TAlk. The resulting source water mass definitions for SLR, SFNS, LADW, and CIL are shown in Table 1 and plotted in Fig. 4. Definitions for the intermediate and deep water masses (CIL, LADW) were derived from data collected during all ten spring/summer cruises, whereas the definition values of the surface-layer water masses (SLR, SFNS), which show higher seasonal and interannual variations, were determined using the same dataset as the model run (May 2016).

2.6 Estimating conservative and non-conservative pCO_2

If waters mix conservatively, the concentration of a particular dissolved constituent can be predicted by a conservative mixing model. Since DIC and TAlk are unaffected by changes in temperature and pressure during closed-system mixing, their conservative concentrations are given by:

$$DIC_{mix} = f_{SLR}DIC_{SLR} + f_{SFNS}DIC_{SFNS} + f_{LADW}DIC_{LADW} + f_{CIL}DIC_{CIL} \quad (10)$$

$$TAlk_{mix} = f_{SLR}TAlk_{SLR} + f_{SFNS}TAlk_{SFNS} + f_{LADW}TAlk_{LADW} + f_{CIL}TAlk_{CIL} \quad (11)$$

where f are the mixing fractions derived from OMP analysis. The conservative pCO_2, pCO_2(mix), was then calculated from DIC_{mix}, $TAlk_{mix}$, *in situ* S_P, and $\overline{SST}$.

Changes in pCO_2 unexplained by water mass mixing, i.e., the non-conservative changes in pCO_2, were estimated as follows:

$$\Delta pCO_2(nonmix) = pCO_2\left(\overline{SST}\right) - pCO_2(mix) \quad (12)$$

where both terms on the right-hand side of the equation are normalized to $\overline{SST}$ in order to remove the effect of temperature on changes in pCO_2. In the context of the present work, ΔpCO_2(nonmix) is treated as a relative value and its calculation assumes that the surface-water temperature does not vary or varies only insignificantly over the sampling period (Burt et al., 2016). After the correction for temperature has been applied,

ΔpCO_2(nonmix) can be mainly attributed to biological activity (photosynthesis, respiration). This is not an unreasonable assumption given the absence of calcium carbonate formation/dissolution in the study area and the negligible effect of air-sea gas exchange on the spatial variability of the mixed-layer DIC (as demonstrated in the results). It should be noted that the nonlinear dependence of the carbonate system on temperature affects the results of equation (12) and that more realistic estimates would be achieved if nonlinear effects were included (Xue et al., 2016).

3 Results and discussion

3.1 Water mass distributions

Fig. 5 and 6 show the mixing fractions (expressed in percentages) of SLR, SFNS, LADW, and CIL throughout the investigated depth range in the Estuary and Gulf of St. Lawrence in May 2016. SLR, LADW, and CIL are important contributors to the water mass structure of the surface mixed layer. As expected, the SLR dominates the mixed layer in the Upper Estuary (between Québec City and Tadoussac). Its relative contribution reaches 100% at the head of the Estuary, where the freshwater runoff from the St. Lawrence River produces a very large seasonal pulse (~15,000 $m^3\ s^{-1}$) during the spring freshet in April–May. The magnitude of the SLR contribution depends strongly on seasonal variations in freshwater runoff, as confirmed by a comparison of the mixed-layer structure at a fixed hydrographic station (Les Escoumins) in May 2011 (~21,925 $m^3\ s^{-1}$), June 2013 (~14,890 $m^3\ s^{-1}$), and May 2016 (~16,393 $m^3\ s^{-1}$). The highest fractions of SLR are found in May 2011, corresponding to the highest monthly mean freshwater runoff recorded during the study period (data provided by the Modelling and Operational Oceanography Division, Canadian Hydrographic Service - Quebec Region, Maurice Lamontagne Institute, Fisheries and Oceans Canada).

Seaward of Tadoussac, the water mass structure of the mixed layer is more complex. The SLR signal becomes diluted with SFNS, LADW, and CIL near the confluence of the Saguenay Fjord and the St. Lawrence Estuary at Tadoussac, which is situated very near a steep sill at the head of the Laurentian Channel. In this zone, internal tides and waves induced by the interaction of the flow field with a rapidly shoaling bottom lead to intense upwelling and mixing of landward-flowing intermediate and deep waters with seaward-flowing Upper Estuary and Saguenay Fjord waters. An upwelling zone is also observed in the region seaward of Pointe-des-Monts, potentially related to the presence of a large anticyclonic eddy centered between Pointe-des-Monts and Rimouski (Ingram and El-Sabh, 1990). In May 2016, the contribution of SFNS was at most ~11% (mean contribution of 3.6%), whereas the mean contributions of LADW and CIL to the

water mass structure of the mixed layer were ~23% and 34%, respectively. Below the mixed layer, the LADW contribution increases rapidly with depth; a core of nearly pure LADW is found at >150m depth in the Lower Estuary and Gulf (along the Laurentian Channel). The highest fractions of CIL can be found in the depth range 30–150 m, although the core of pure CIL is less pronounced in comparison with the intrusion of nearly pure LADW.

3.2 Biologically-induced concentration changes

Also available from the model output are the estimated changes in dissolved oxygen, nutrient, and inorganic carbon concentrations due to *in situ* biological activity (photosynthesis, respiration). The amount of ΔDIC_{bio} was revealed by relating the variable ΔP to the C:P ratio ($\pm r_{C/P}$), as shown in equation (7). Positive values of ΔDIC_{bio} indicate DIC addition due to net respiration, whereas negative values indicate DIC removal due to net photosynthesis. Fig. 7 shows the estimated ΔDIC_{bio} and the AOU calculated from equation (6) throughout the water column of the study area. The influence of biological activity is clearly discriminated in the surface mixed layer and the deep layer (depth >150 m), with the distribution pattern of ΔDIC_{bio} matching that of AOU. The ΔDIC_{bio} is linearly correlated with the AOU in both the surface mixed (R^2 = 0.87) and deep (R^2 = 0.77) layers (see Fig. 8). The regressions yielded a ΔDIC_{bio}/AOU of ~0.9 in the mixed layer and ~0.74 in the deep layer, in good agreement with the C:–O_2 Redfield ratio of ~0.77.

In the deep waters of the study area, the ΔDIC_{bio} estimates are always positive and increase in a landward direction. This is consistent with evidence that the products of organic matter decomposition (metabolites: DIC and nutrients) increase with depth and toward the head of the Laurentian Channel, as the deep layer of LADW flows sluggishly from Cabot Strait into the Lower Estuary (Coote and Yeats, 1979). Within the surface mixed layer, the ΔDIC_{bio} values generally decrease from positive to negative in a seaward direction (see Fig. 9), the pattern being consistent with the general progression from chemical distributions controlled by mixing/estuarine processes in the Upper Estuary to those controlled by biological/oceanic processes in the Lower Estuary (Yeats, 1990). The latter is the region of the St. Lawrence with the most favorable conditions for phytoplankton growth (e.g., low turbidity, continued availability of excess nutrients, enhanced water column stability). The location of the ΔDIC_{bio} minima (near Pointe-des-Monts in the vicinity of the anticyclonic eddy) corresponds to a zone of maximal productivity (over the downstream portion of the Lower Estuary; Savenkoff et al., 1994) resulting from the mixing of nutrient-rich waters, upwelled at the head of the Laurentian Channel, with warmer freshwaters flowing in from the north-shore rivers.

3.3 DIC budget in the water column

Table 2 shows the DIC budget (DIC_{mix}, ΔDIC_{bio}, ΔDIC_{gas}) in the surface mixed layer for three important sub-regions of the St. Lawrence system: (1) the shallow Upper Estuary, (2) the deep Lower Estuary, and (3) the open Gulf. The major components of the DIC budget in the deep layer (depth >150 m) are included for comparison. It is clear that mixing (e.g., internal tides, horizontal advection, upwelling, internal waves, eddies) is the dominant contributor to the DIC budget throughout the St. Lawrence, accounting for >98% (surface mixed layer) and >95% (deep layer) of the observed variability in DIC. Within the mixed layer, the DIC_{mix} estimates range from 1082 μmol kg^{-1} in the relatively fresh waters of the Upper Estuary to 2052 μmol kg^{-1} in the marine waters of the Lower Estuary and Gulf. As expected from its sluggish flow (~0.5 cm s^{-1}; Bugden, 1988), the DIC_{mix} estimates in the deep layer are approximately constant (2184 ± 14.2 μmol kg^{-1}), indicating that the deep water of the Laurentian Channel travels landward without mixing with other water masses.

The contributions of biological activity and gas exchange to the DIC budget are quite small compared to that of mixing. Biological processes account for –8.3 to 1.5% (surface mixed layer) and 1.5 to 5.1% (deep layer) of the observed variability in DIC. As expected in the mixed layer, the ΔDIC_{bio} maxima (26.7 μmol kg^{-1}; net respiration) and minima (–143.4 μmol kg^{-1}; net photosynthesis) occur, respectively, in the river-dominated (Upper Estuary) and marine-dominated (Lower Estuary and Gulf) regions. In the deep layer, the ΔDIC_{bio} values are always positive (ΔDIC_{bio} = 32.4 to 141.0 μmol kg^{-1}) and increase from the Gulf to the Lower Estuary, owing to the accumulation of metabolites. Air-sea gas exchange is responsible for approximately –0.49% of the DIC variability in the surface mixed layer. The mean value of ΔDIC_{gas} calculated from equation (3) is 0.72 ± 4.2 μmol kg^{-1}, whereas the mean value from equation (4) is –13.3 ± 40.7 μmol kg^{-1}. These estimates are quite uncertain. While the two approaches represent important preliminary steps in quantifying ΔDIC_{gas}, neither is wholly satisfactory. The former may underestimate ΔDIC_{gas}, as $\Delta DIC_{gas,eqn3}$ is equivalent to the DIC residual, R_{DIC}, in equation (7). On the other hand, the latter may lead to a practical upper limit on ΔDIC_{gas}, since, on the time scale of the residence time of surface waters in the study area (~4 months), the mixed-layer DIC budget is more likely to be influenced by mixing and biological processes than by gas exchange at the air-sea interface (time scale of several months to ~1 year).

Although the amount of DIC added or removed by biological activity is small compared with the input of DIC by advection and mixing, the ΔDIC_{bio} is disproportionately important to surface-water pCO_2 dynamics. In contrast to the DIC_{mix},

the biologically-induced change in DIC is not accompanied by a significant, concomitant change in TAlk, meaning that the ΔDIC_{bio} has an important impact on the buffering capacity (DIC:TAlk ratio) of mixed-layer waters. The DIC:TAlk ratio partially determines the fraction of DIC that can escape to the atmosphere in the form of free dissolved CO_2 (i.e., the excess DIC; see Abril et al., 2000; Borges, 2011). We define the excess DIC (CO_2^*) as the difference between the observed DIC and a theoretical DIC at atmospheric equilibrium. The latter was calculated from the measured TAlk and the mean atmospheric pCO_2 in May 2016 (~405 µatm). As shown in Fig. 10, when the CO_2^* is plotted against the ΔDIC_{bio}, an excellent correlation ($R^2 = 0.96$) is found; the slope of the line is close to 1 (0.98). The linearity in the CO_2^* versus ΔDIC_{bio} relationship suggests that the departure of DIC from atmospheric equilibrium is mainly the result of biological processes (photosynthesis, respiration). These results must be interpreted with caution, since excess DIC may originate from other processes that occur on relatively short time scales (weeks) (e.g., freshwater fluxes, water mass mixing) (Burt et al., 2016). Nevertheless, we conclude from the 1:1 relationship between CO_2^* and ΔDIC_{bio} that biological activity controls excess DIC in the surface mixed layer of the St. Lawrence Estuary and Gulf.

3.4 Controls on the spatial variability of pCO_2

The distributions of pCO_2(obs), $pCO_2(\overline{SST})$, pCO_2(mix), ΔpCO_2(nonmix), and ΔpCO_2(temp) in the surface mixed layer of the study area are shown in Fig. 11. Values of pCO_2(obs) range from ~139 to 703 µatm (in contrast, atmospheric pCO_2 was ~405 µatm in May 2016), with mixed-layer waters shifting from pCO_2 supersaturation (local CO_2 source) to pCO_2 undersaturation (local CO_2 sink) in the downstream portion of the Lower Estuary. After correcting for temperature, the observed variability in the $pCO_2(\overline{SST})$ distribution (~147 to 645 µatm) reflects both mixing and biological processes, but the dominant, underlying process remains to be identified. The distribution of pCO_2(mix) is relatively uniform spatially (standard deviation of ±32.3 µatm), suggesting that water mass mixing contributes little to the spatial changes in $pCO_2(\overline{SST})$. Likewise, temperature differences (due to warming or cooling) contribute minimally to the spatial variability of pCO_2 (ΔpCO_2(temp) = –85.9 to 66.7 µatm). In contrast, biological activity appears to exert a major control on the $pCO_2(\overline{SST})$ distribution. The distribution pattern of ΔpCO_2(nonmix) is roughly bimodal with peaks in the landward (182.2 µatm) and seaward (–342.2 µatm) portions of the study area, consistent with the ΔDIC_{bio} distribution.

The spatial variability of temperature-normalized pCO_2 in the coastal ocean can be characterized by two important drivers: (1) the change of DIC by *in situ* biological

processes and (2) the inputs of DIC and TAlk by freshwater and seawater mixing. In this study, the externally supplied DIC and TAlk could be broken down into riverine (DIC_{river}, $TAlk_{river}$) and marine (DIC_{marine}, $TAlk_{marine}$) inputs as follows:

$$DIC_{river} = f_{SLR}DIC_{SLR} + f_{SFNS}DIC_{SFNS} \quad (13)$$

$$TAlk_{river} = f_{SLR}TAlk_{SLR} + f_{SFNS}TAlk_{SFNS} \quad (14)$$

$$DIC_{marine} = f_{LADW}DIC_{LADW} + f_{CIL}DIC_{CIL} \quad (15)$$

$$TAlk_{marine} = f_{LADW}TAlk_{LADW} + f_{CIL}TAlk_{CIL} \quad (16)$$

where the sum of DIC_{river} and DIC_{marine} is equivalent to DIC_{mix} (equation 10) and the sum of $TAlk_{river}$ and $TAlk_{marine}$ is equivalent to $TAlk_{mix}$ (equation 11). While the approach we have taken is conceptually similar to the two-end-member mixing model used by Jiang et al. (2008) to estimate riverine and marine inputs, ours is a more rigorous attempt given the application of OMP analysis.

The ΔDIC_{bio}, $DIC_{river}/TAlk_{river}$, and $DIC_{marine}/TAlk_{marine}$ must be invoked if the observed $pCO_2(\overline{SST})$ variability in our study area is to be explained (Fig. 12). We assume here that ΔDIC_{bio} depends only on the change in DIC due to organic matter production/decomposition (photosynthesis/respiration) since calcium carbonate formation/dissolution is insignificant in the St. Lawrence system. Based on the strong correlation between $pCO_2(\overline{SST})$ and ΔDIC_{bio} (R^2 = 0.92), photosynthesis/respiration appears to be the major driver of spatial variations in $pCO_2(\overline{SST})$. This is consistent with (1) the earlier observation that the excess DIC (DIC loss) in the surface mixed layer of the St. Lawrence Estuary and Gulf is likely the result of *in situ* respiration (biological drawdown) and (2) the finding that the net CO_2 flux in estuaries with long water residence times, such as the St. Lawrence, results from the balance between autotrophy and heterotrophy (Borges and Abril, 2011).

Although multi-tracer, quantitative water mass analysis has yielded convincing evidence that biological activity is linked to the spatial variability of pCO_2, an additional line of evidence is worth mentioning. The contributions of organic matter production/decomposition, calcium carbonate formation/dissolution, and air-sea gas exchange to spatial changes in $pCO_2(\overline{SST})$ can be assessed from the concomitant change

of DIC and TAlk associated with these processes. The dominant role of biological activity in altering the inorganic carbon concentrations becomes apparent after corrections are applied for the effect of water mass mixing (see Fig. 13). A comparison of the slopes of the least-squares fit to the data (black line) and the linear relationship for photosynthesis/respiration (green line) provides a rough estimate of the relative contribution of biological activity. To minimize the influence of outliers, the data were fitted using robust least-squares regression. Assuming that the change in DIC and TAlk (TAlk/DIC) due to biological activity is -0.21, its contribution to the spatial distribution of DIC and TAlk in the St. Lawrence is estimated to be at least ~60%, while it is likely that gas exchange and model errors are responsible for some fraction of the remainder.

In addition to *in situ* biological activity, lateral transport of inorganic carbon contributes to net CO_2 fluxes in the coastal ocean. Owing to the lower buffering capacity of freshwater compared to seawater, approximately 10% of the CO_2 emissions from inner estuaries can be attributed to the ventilation of riverine CO_2 (Borges et al., 2006). Fig. 14 (left) shows the DIC:TAlk ratio in the surface mixed layer of the St. Lawrence as a function of the percent contribution of riverine and marine waters. The DIC:TAlk ratio is >1 when the mixed layer is dominated by freshwater inputs (SLR, SFNS) and decreases with the increasing contribution of seawater (LADW, CIL). Although the mixed-layer inorganic carbon budget depends strongly on the mixing fractions (contributions) of freshwater and seawater, other processes appear to be more important in modifying the DIC:TAlk ratio and its relation to $pCO_2(\overline{SST})$, particularly in the drawdown of DIC and pCO_2 at higher seawater:freshwater ratios (Fig. 14, right). Moreover, the lack of correlation between $pCO_2(\overline{SST})$ and inputs of riverine- and marine-derived DIC and TAlk (see Fig. 12) suggests that freshwater and seawater mixing is not an important driver of spatial changes in $pCO_2(\overline{SST})$. Therefore, considering that spatial variations in temperature account for only –0.56% (±8.4%) of the observed pCO_2 variability during the 2016 sampling period, one can conclude that biological activity is the dominant control on surface-water pCO_2 dynamics in the St. Lawrence, explaining the shift from pCO_2 supersaturation (estuarine region) to pCO_2 undersaturation (maritime region).

4 Summary and conclusions

Quantitative water mass analysis (such as OMP analysis) is now a standard tool in oceanography for the description of water mass structures and is capable of resolving the effects of both mixing and remineralization processes on observed tracer fields. In this paper, a further extension of the OMP analysis method is presented which accounts for phytoplankton photosynthesis by incorporating the concept of apparent oxygen

utilization (AOU), offering new opportunities for its implementation. The improved method is validated by its successful application to hydrographic, nutrient, and inorganic carbon data in the surface mixed layer of the Estuary and Gulf of St. Lawrence, a large-scale estuarine system representative of the more general coastal environment. The method is utilized to quantify the effects of water mass mixing, biological activity, and gas exchange on DIC observations. It has been shown that by analyzing the DIC budget (DIC_{mix}, ΔDIC_{bio}, ΔDIC_{gas}) in conjunction with the temperature-normalized pCO_2, it is possible to differentiate between the physical and biological drivers affecting pCO_2 changes in the coastal environment. The results clearly demonstrate that biological activity is responsible for the upstream to downstream shift from pCO_2 supersaturation (net heterotrophy) to pCO_2 undersaturation (net autotrophy) along the St. Lawrence land—ocean continuum.

This work establishes the potential of multi-tracer, quantitative water mass analysis in coastal carbon research. Its limitations include the shortage of suitable hydrographic properties in space and time and the seasonal and interannual variability of water mass properties in the surface mixed layer. The method could certainly be improved by including additional conservative tracers such as stable isotopes (e.g., the stable hydrogen isotopic composition of water) and CFC concentrations. Nonetheless, the robustness of the results presented here (the mass conservation residual was, at most, 0.73%) indicates that extended OMP analysis is a powerful technique to elucidate the underlying physical and biogeochemical processes controlling inorganic carbon and CO_2 fluxes in the coastal ocean.

Data availability. A MATLAB program for the OMP analysis method used in this work has been developed and is available upon request from the first author (ashley.dinauer@mail.mcgill.ca).

Author contribution. A.D. and A.M. conceived the project. A.M. acquired and processed the data prior to 2016. A.D. conducted the data analysis and wrote the first draft of the paper whereas A.M. provided editorial and scientific recommendations.

Competing interests. The authors declare that they have no conflict of interest.

Acknowledgements. We wish to thank the Captains and crews of the R/V *Coriolis II* for their unwavering help over the years. We also wish to acknowledge Gilles Desmeules and Michel Rousseau for their dedicated electronic and field sampling support as well as Constance Guignard for her help in cruise preparation and

field data acquisition. Most of the data were acquired opportunistically on research cruises funded by grants to A.M. or Canadian colleagues by the Natural Sciences and Engineering Research Council of Canada (NSERC). The work was funded by a Regroupement Stratégique grant from the Fonds Québécois de Recherche Nature et Technologies (FQRNT) to GEOTOP as well as NSERC Discovery and MEOPAR grants to A.M. A.D. wishes to thank MEOPAR and the Department of Earth and Planetary Sciences at McGill for financial support in the form of stipends, scholarships and assistantships.

References

Abril, G., H. Etcheber, A. V. Borges, and M. Frankignoulle. 2000. Excess atmospheric carbon dioxide transported by rivers into the Scheldt estuary. Cr. Acad. Sci. II A. 330: 761–768.

Anderson, L. A., and J. L. Sarmiento. 1994. Redfield ratios of remineralization determined by nutrient data analysis. Global Biogeochem. Cy. 8: 65–80.

Bauer, J. E., W. J. Cai, P. A. Raymond, T. S. Bianchi, C. S. Hopkinson, and P. A. Regnier. 2013. The changing carbon cycle of the coastal ocean. Nature 504: 61–70.

Benson, B. B., and D. Krause. 1984. The concentration and isotopic fractionation of oxygen dissolved in freshwater and seawater in equilibrium with the atmosphere. Limnol. Oceanogr. 29: 620–632.

Borges, A. V. 2011. Present day carbon dioxide fluxes in the coastal ocean and possible feedbacks under global change. In: P. Duarte and J. M. Santana-Casiano (Eds.), Oceans and the atmospheric carbon content. Springer Science+Business Media B.V., pp. 47–77.

Borges, A. V., and G. Abril. 2011. Carbon dioxide and methane dynamics in estuaries. In: E. Wolanski and D. S. McLusky (Eds.), Treatise on estuarine and coastal science. Academic Press, pp. 119–161.

Borges, A. V., L. S. Schiettecatte, G. Abril, B. Delille, and F. Gazeau. 2006. Carbon dioxide in European coastal waters. Estuar. Coast. Shelf Sci. 70: 375–387.

Broecker, W. S., and T.-H. Peng. 1982. Tracers in the Sea. Lamont-Doherty Geological Observatory, Columbia University, Palisades, NY, 690 pp.

Bugden, G. L. 1988. Oceanographic conditions in the deeper waters of the Gulf of St. Lawrence in relation to local and oceanic forcing. NAFO SCR document, 88/87.

Burt, W. J., H. Thomas, M. Hagens, J. Pätsch, N. M. Clargo, L. A. Salt, V. Winde, and M. E. Böttcher. 2016. Carbon sources in the North Sea evaluated by means of radium and stable carbon isotope tracers. Limnol. Oceanogr. 61: 666–683.

Cai, W. J., and Y. Wang. 1998. The chemistry, fluxes, and sources of carbon dioxide in the estuarine waters of the Satilla and Altamaha Rivers, Georgia. Limnol. Oceanogr. 43: 657–668.

Cantin, G., M. Levasseur, M. Gosselin, and S. Michaud. 1996. Role of zooplankton in the mesoscale distribution of surface dimethylsulfide concentrations in the Gulf of St. Lawrence, Canada. Mar. Ecol.-Prog. Ser. 141: 103–117.

Coote, A. R., and P. A. Yeats. 1979. Distribution of nutrients in the Gulf of St. Lawrence. J. Fish. Res. Board Can. 36: 122–131.

d'Anglejan, B. 1990. Recent sediments and sediment transport processes in the St. Lawrence Estuary. In: M. I. El-Sabh and N. Silverberg (Eds.), Oceanography of a large-scale estuarine system. Springer-Verlag, pp. 109–129.

de Boyer Montégut, C., G. Madec, A. S. Fischer, A. Lazar, and D. Iudicone. 2004. Mixed layer depth over the global ocean: An examination of profile data and a profile-based climatology. J. Geophys. Res. 109: C12003, doi:10.1029/2004JC002378.

Devine, L., S. Plourde, M. Starr, J.-F. St-Pierre, L. St-Amand, P. Joly, and P. S. Galbraith. 2015. Chemical and biological oceanographic conditions in the Estuary and Gulf of St. Lawrence during 2013. DFO Can. Sci. Advis. Sec. Res. Doc., 2015/013, 45 pp.

Dinauer, A., and A. Mucci. 2017. Spatial variability in surface-water pCO_2 and gas exchange in the world's largest semi-enclosed estuarine system: St. Lawrence Estuary (Canada). Biogeosciences 14: 3221–3237.

Doney, S. C., V. J. Fabry, R. A. Feely, and J. A. Kleypas. 2009. Ocean acidification: the other CO_2 problem. Annu. Rev. Mar. Sci. 1: 169–192.

Dufour, R., and P. Ouellet. 2007. Estuary and Gulf of St. Lawrence marine ecosystem overview and assessment report. Can. Tech. Rep. Fish. Aquat. Sci., 2744E, 112 pp.

El-Sabh, M. I., and N. Silverberg. 1990. The St. Lawrence Estuary: introduction. In: M. I. El-Sabh and N. Silverberg (Eds.), Oceanography of a large-scale estuarine system. Springer-Verlag, pp. 1–9.

Fassbender, A. J., C. L. Sabine, and K. M. Feifel. 2016. Consideration of coastal carbonate chemistry in understanding biological calcification. Geophys. Res. Lett. 43: 4467–4476.

Galbraith, P. S. 2006. Winter water masses in the Gulf of St. Lawrence. J. Geophys. Res. 111: C06022, doi:10.1029/2005JC003159.

Gattuso, J.-P., M. Frankignoulle, and R. Wollast. 1998. Carbon and carbonate metabolism in coastal aquatic ecosystems. Annu. Rev. Ecol. Syst. 29: 405–434.

Gilbert, D., B. Sundby, C. Gobeil, A. Mucci, and G. H. Tremblay. 2005. A seventy-two-year record of diminishing deep-water oxygen in the St. Lawrence estuary: The northwest Atlantic connection. Limnol. Oceanogr. 50: 1654–1666.

Grasshoff, K., K. Kremling, and M. Ehrhardt. 1999. Methods of seawater analysis, third ed. Wiley-VCH.

Gratton, Y., G. Mertz, and J. A. Gagné. 1988. Satellite observations of tidal upwelling and mixing in the St. Lawrence Estuary. J. Geophys. Res.-Oceans 93: 6947–6954.

Hedges, J. I., J. A. Baldock, Y. Gélinas, C. Lee, M. L. Peterson, and S. G. Wakeham. 2002. The biochemical and elemental compositions of marine plankton: A NMR perspective. Mar. Chem. 78: 47–63.

Hupe, A., and J. Karstensen. 2000. Redfield stoichiometry in Arabian Sea subsurface waters. Global Biogeochem. Cy. 14: 357–372.

Ingram, R. G., and M. I. El-Sabh. 1990. Fronts and mesoscale features in the St. Lawrence Estuary. In: M. I. El-Sabh and N. Silverberg (Eds.), Oceanography of a large-scale estuarine system. Springer-Verlag, pp. 71–93.

Ito, T., M. J. Follows, and E. A. Boyle. 2004. Is AOU a good measure of respiration in the oceans? Geophys. Res. Lett. 31: L17305, doi:10.1029/2004GL020900.

Jiang, L. Q., W. J. Cai, and Y. Wang. 2008. A comparative study of carbon dioxide degassing in river-and marine-dominated estuaries. Limnol. Oceanogr. 53: 2603–2615.

Karstensen, J., and M. Tomczak. 1998. Age determination of mixed water masses using CFC and oxygen data. J. Geophys. Res.-Oceans 103: 18599–18609.

Levasseur, M., M. D. Keller, E. Bonneau, D. D'Amours, and W. K. Bellows. 1994. Oceanographic basis of a DMS-related Atlantic cod (Gadus morhua) fishery problem: blackberry feed. Can. J. Fish. Aquat. Sci. 51: 881–889.

Levasseur, M., S. Sharma, G. Cantin, S. Michaud, M. Gosselin, and L. Barrie. 1997. Biogenic sulfur emissions from the Gulf of Saint Lawrence and assessment of its impact on the Canadian east coast. J. Geophys. Res.-Atmos. 102: 28025–28039.

McDougall, T. J., and P. M. Barker. 2011. Getting started with TEOS-10 and the Gibbs Seawater (GSW) Oceanographic Toolbox. SCOR/IAPSO WG127, ISBN 978-0-646-55621-5, 28 pp.

Orr, J. C., J.-M. Epitalon, A. G. Dickson, and J.-P. Gattuso. 2017. Routine uncertainty propagation for the marine carbon dioxide system. In prep. for Mar. Chem., 2017.

Poole, R., and M. Tomczak. 1999. Optimum multiparameter analysis of the water mass structure in the Atlantic Ocean thermocline. Deep-Sea Res. Pt. I 46: 1895–1921.

Redfield, A. C., B. H. Ketchum, and F. A. Richards. 1963. The influence of organisms on the composition of seawater. In: M. N. Hill (Ed.), The sea. Interscience, pp. 26–77.

Sabine, C. L., and R. A. Feely. 2007. The oceanic sink for carbon dioxide. In: D. Reay, N. Hewitt, J. Grace, and K. Smith (Eds.), Greenhouse gas sinks. CABI Publishing, pp. 31–49.

Sabine, C. L., and R. M. Key. 1998. Controls on fCO_2 in the South Pacific. Mar. Chem. 60: 95–110.

Saucier, F. J., and J. Chassé. 2000. Tidal circulation and buoyancy effects in the St. Lawrence Estuary. Atmos. Ocean 38: 505–556.

Saucier, F. J., F. Roy, D. Gilbert, P. Pellerin, and H. Ritchie. 2003. Modeling the formation and circulation processes of water masses and sea ice in the Gulf of St. Lawrence. Canada. J. Geophys. Res. 108: 3269, doi:10.1029/2000JC000686.

Savenkoff, C., L. Comeau, A. F. Vézina, and Y. Gratton. 1994. Seasonal variation of the biological activity in the lower St. Lawrence Estuary. Can. Tech. Rep. Fish. Aquat. Sci., 2006, 22 pp.

Schneider, B., J. Karstensen, A. Oschlies, and R. Schlitzer. 2005. Model-based evaluation of methods to determine C:N and N:P regeneration ratios from dissolved nutrients. Global Biogeochem. Cy. 19: GB2009, doi:10.1029/2004GB002256.

Silverberg, N., and B. Sundby. 1990. Sediment-water interaction and early diagenesis in the Laurentian Trough. In: M. I. El-Sabh and N. Silverberg (Eds.), Oceanography of a large-scale estuarine system. Springer-Verlag, pp. 202–238.

Simons, R. D., S. G. Monismith, F. J. Saucier, L. E. Johnson, and G. Winkler. 2010. Modelling stratification and baroclinic flow in the estuarine transition zone of the St. Lawrence estuary. Atmos.-Ocean 48: 132–146.

Takahashi, T., J. Olafsson, J. G. Goddard, D. W. Chipman, and S. C. Sutherland. 1993. Seasonal variation of CO_2 and nutrients in the high-latitude surface oceans: a comparative study. Global Biogeochem. Cy. 7: 843–878.

Tee, K-T. 1990. Meteorologically and buoyancy induced subtidal salinity and velocity variations in the St. Lawrence Estuary. In: M. I. El-Sabh and N. Silverberg (Eds.), Oceanography of a large-scale estuarine system. Springer-Verlag, pp. 51–70.

Tomczak, M. 1981. A multi-parameter extension of temperature/salinity diagram techniques for the analysis of non-isopycnal mixing. Prog. Oceanogr. 10: 147–171.

Tomczak, M. 1999. Some historical, theoretical and applied aspects of quantitative water mass analysis. J. Mar. Res. 57: 275–303.

Tomczak, M., and D. G. Large. 1989. Optimum multiparameter analysis of mixing in the thermocline of the eastern Indian Ocean. J. Geophys. Res.-Oceans 94: 16141–16149.

van Heuven, S., D. Pierrot, J. W. B. Rae, E. Lewis, and D. W. R. Wallace. 2011. MATLAB program developed for CO_2 system calculations. ORNL/CDIAC-105b, Carbon Dioxide Information Analysis Center, Oak Ridge National Laboratory, U.S. Department of Energy, Oak Ridge, Tennessee, doi:10.3334/CDIAC/otg.CO2SYS_MATLAB_v1.1.

Weiss, R. 1974. Carbon dioxide in water and seawater: the solubility of a non-ideal gas. Mar. Chem. 2: 203–215.

Xue, L., W.-J. Cai, X. Hu, C. Sabine, S. Jones, A. J. Sutton, L.-Q. Jiang, and J. J. Reimer. 2016. Sea surface carbon dioxide at the Georgia time series site (2006–2007): Air–sea flux and controlling processes. Prog. Oceanogr. 140: 14–26.

Yeats, P. A. 1990. Reactivity and transport of nutrients and metals in the St. Lawrence Estuary. In: M. I. El-Sabh and N. Silverberg (Eds.), Oceanography of a large-scale estuarine system. Springer-Verlag, pp. 155–169.

Table 1. Source water mass definitions for St. Lawrence River (SLR), Saguenay Fjord and north-shore rivers (SFNS), Labrador/Atlantic deep water (LADW), and Gulf summertime cold intermediate layer (CIL).

Property	SLR	SFNS	LADW	CIL
Temperature (°C)	**10.1** ± 0.38	**4.25** ± 0.06	**7.79** ± 1.4	**-0.61** ± 0.18
Salinity (S_P)	**0.00** ± 0	**0.00** ± 0	**34.9** ± 0.24	**32.2** ± 0.52
$\delta^{18}O_{water}$ (‰)	**-9.39** ± 0.08	**-13.3** ± 0.15	**-0.09** ± 0.05	**-1.51** ± 0.59
Oxygen (µmol kg^{-1})	**352** ± 4.1	**433** ± 2.4	**156** ± 13.9	**335** ± 24.2
SRP (µmol kg^{-1})	**1.05** ± 0.21	**0.12** ± 0.03	**1.54** ± 0.12	**0.95** ± 0.09
Nitrate (µmol kg^{-1})	**25.5** ± 0.14	**9.47** ± 0.23	**22.1** ± 2.3	**7.44** ± 1.7
Silicate (µmol kg^{-1})	**38.6** ± 1.2	**85.4** ± 1.0	**14.9** ± 4.3	**5.85** ± 1.1
DIC (µmol kg^{-1})	**1105** ± 30.3	**220** ± 0	**2203** ± 16.5	**2099** ± 10.1
TAlk (µmol kg^{-1})	**1081** ± 30.2	**186** ± 0	**2310** ± 15.1	**2181** ± 24.1

Table 2. The regionally averaged DIC_{mix}, ΔDIC_{bio}, and ΔDIC_{gas} in the surface mixed layer and the deep layer (depth >150 m) of the Upper Estuary (Île d'Orléans to Tadoussac), Lower Estuary (Tadoussac to Pointe-des-Monts), and Gulf (seaward of Pointe-des-Monts).

	Mixed layer			Deep layer		
	Upper	Lower	Gulf	Upper	Lower	Gulf
DIC_{mix}	**1368** ± 273	**1878** ± 71	**1949** ± 84	–	**2181** ± 15	**2189** ± 12
ΔDIC_{bio}	**11.7** ± 10	**-26.9** ± 47	**-80.8** ± 14	–	**98.3** ± 25	**69.8** ± 17
$\Delta DIC_{gas,eqn3}$	**2.3** ± 6	**-0.85** ± 2	**0.21** ± 1	–	–	–
$\Delta DIC_{gas,eqn4}$	**-43.2** ± 12	**4.3** ± 52	**25.6** ± 8	–	–	–

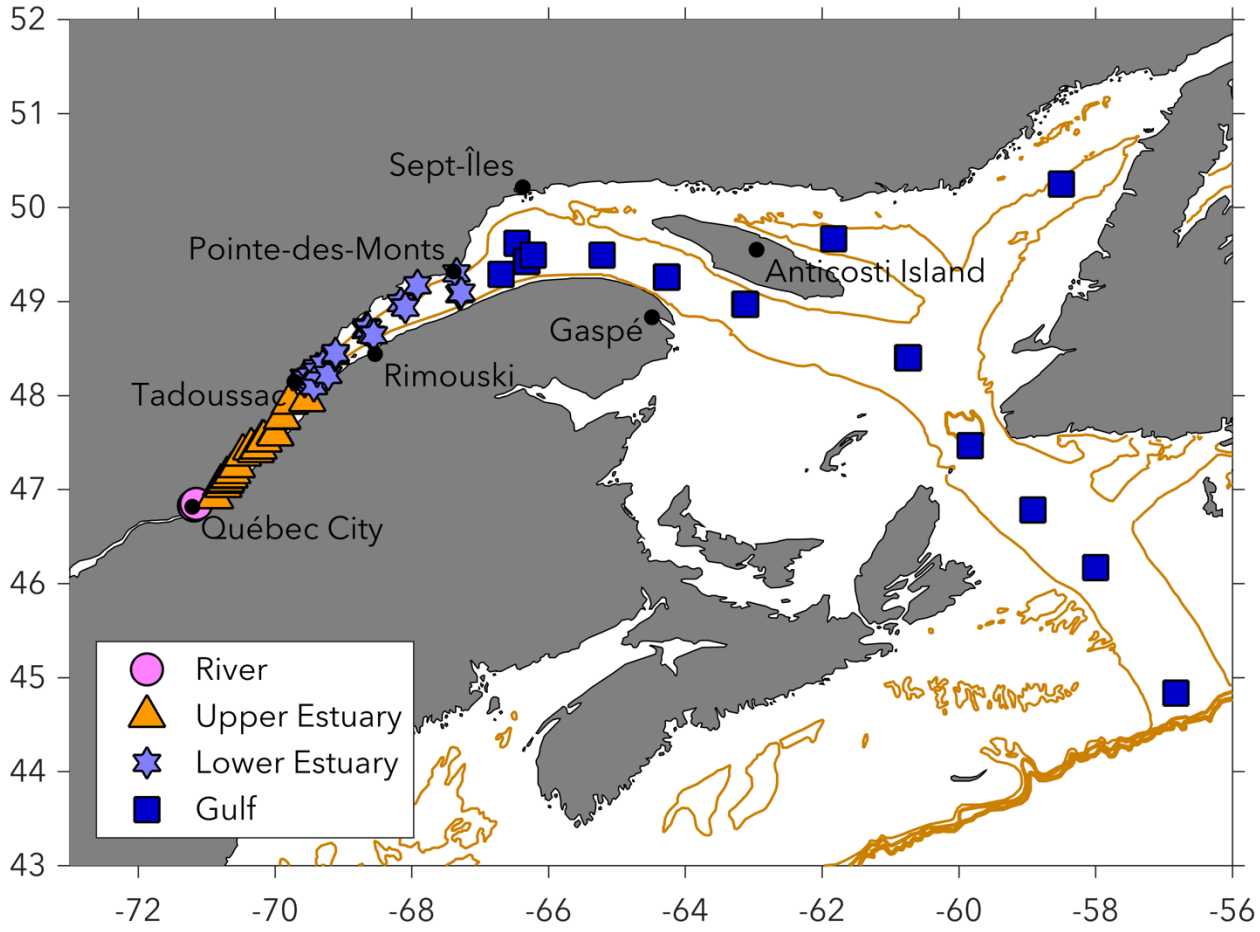

Figure 1. Map of hydrographic stations for the R/V *Coriolis II* cruises (July 2003, June 2006, May 2007, July 2007, June 2009, July 2009, July 2010, May 2011, June 2013, and May 2016). Symbols show the four principal subdivisions of the St. Lawrence land–ocean continuum: River (circle), Upper Estuary (triangle), Lower Estuary (star), and Gulf (square). The solid gold line follows the 200m isobath of the Laurentian Channel. The OMP analysis method was applied to the set of observations from May 2016. The source water mass definitions for the intermediate and deep water masses were based on data from all cruises.

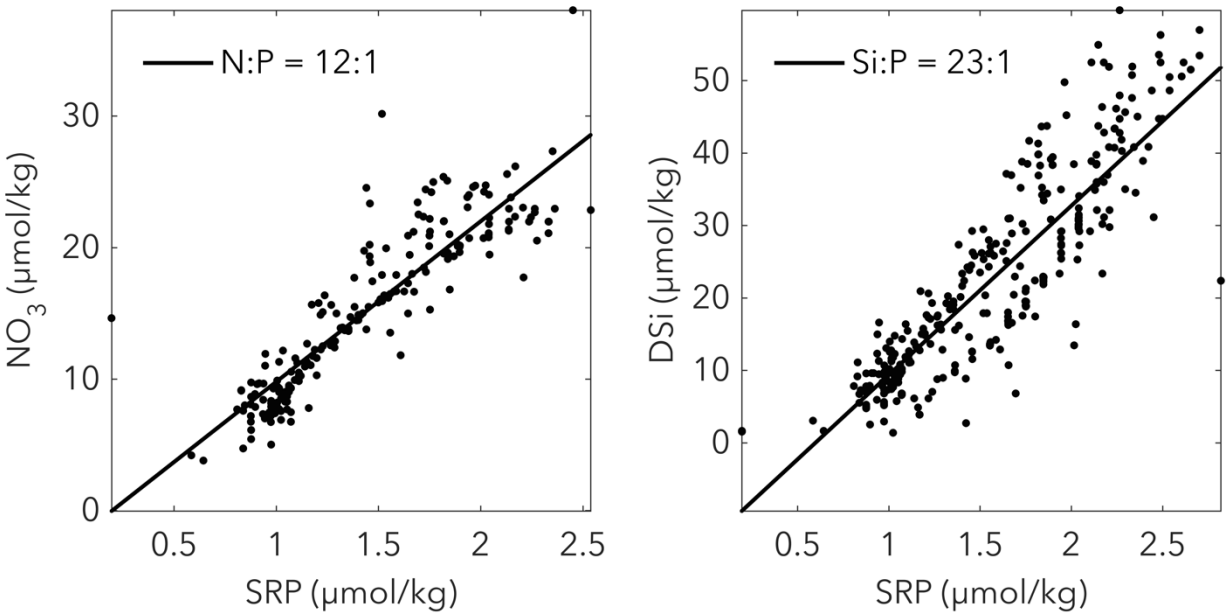

Figure 2. Correlation between (i) NO_3 and SRP and (ii) DSi and SRP for all samples on stations deeper than 30 m. Note that, based on results from the June 2013 cruise, the nitrite and ammonium concentrations are extremely low, with mean values of ~0.20 µmol kg^{-1} and ~0.86 µmol kg^{-1}, respectively.

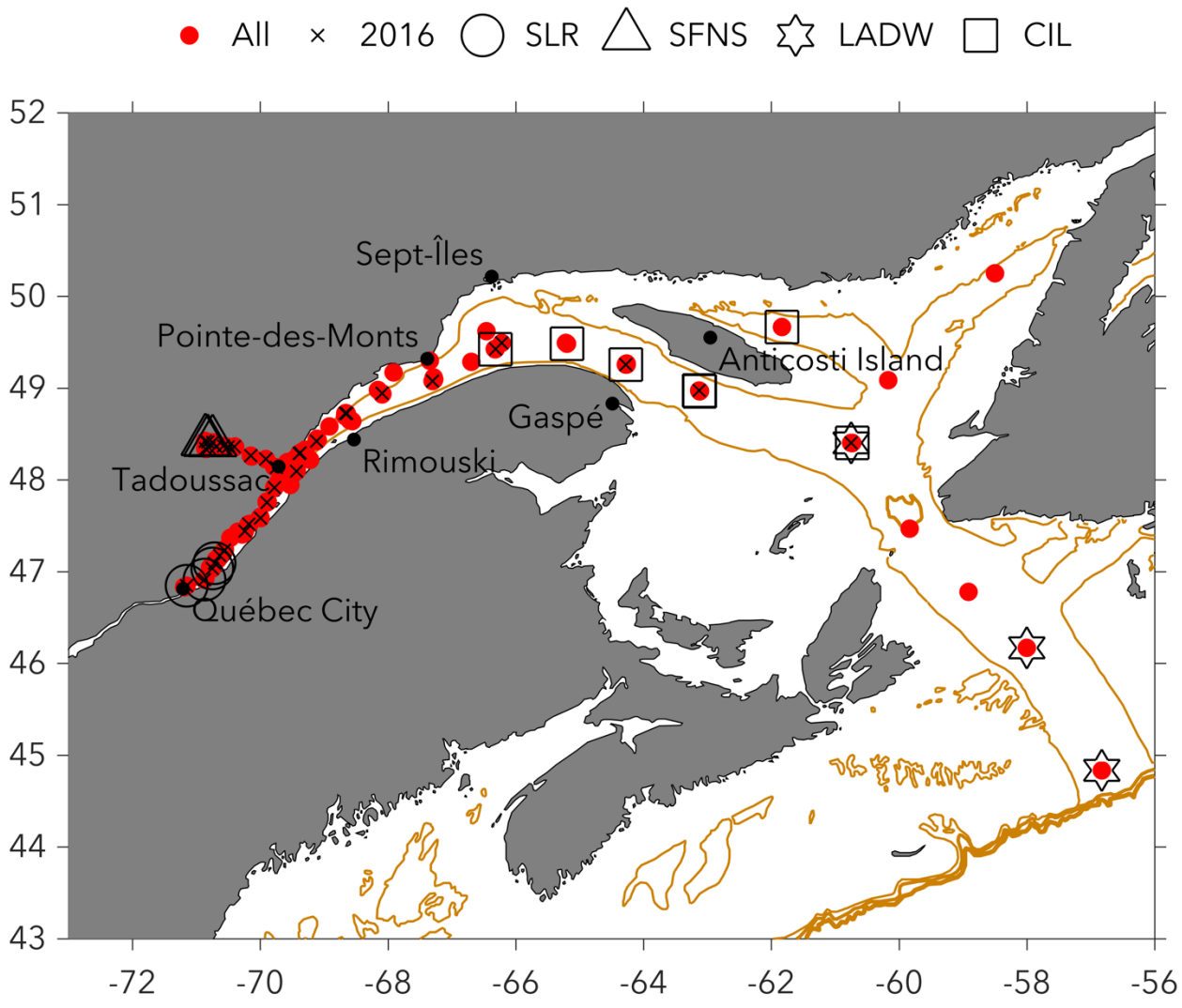

Figure 3. Hydrographic stations used to define the water mass properties of the four major source water masses considered in the OMP analysis: St. Lawrence River (SLR), Saguenay Fjord and north-shore rivers (SFNS), Labrador/Atlantic deep water (LADW), and Gulf summertime cold intermediate layer (CIL).

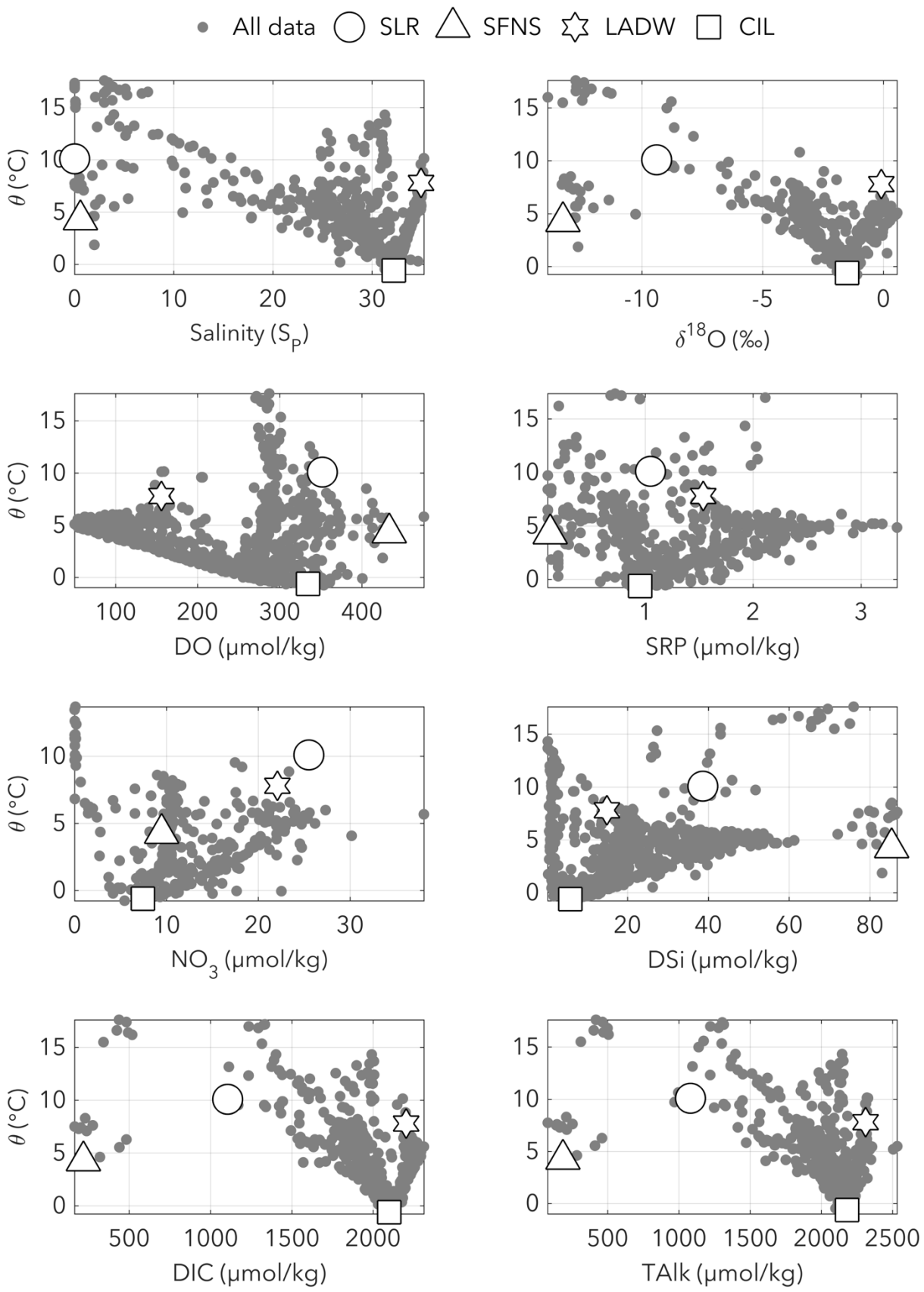
All data
SLR
SFNS
LADW
CIL
θ (°C)
Salinity (S_P)
δ18O (‰)
DO (µmol/kg)
SRP (µmol/kg)
NO3 (µmol/kg)
DSi (µmol/kg)
DIC (µmol/kg)
TAlk (µmol/kg)

1161

Figure 4. Potential temperature versus (i) salinity, (ii) $\delta^{18}O_{water}$, (iii) oxygen, (iv) SRP, (v) nitrate, (vi) silicate, (vii) DIC, and (viii) TAlk for all ten R/V *Coriolis II* cruises. The source water masses are indicated as open symbols: circle, St. Lawrence River (SLR); triangle, Saguenay Fjord and north-shore rivers (SFNS); star, Labrador/Atlantic deep water (LADW); square, Gulf summertime cold intermediate layer (CIL).

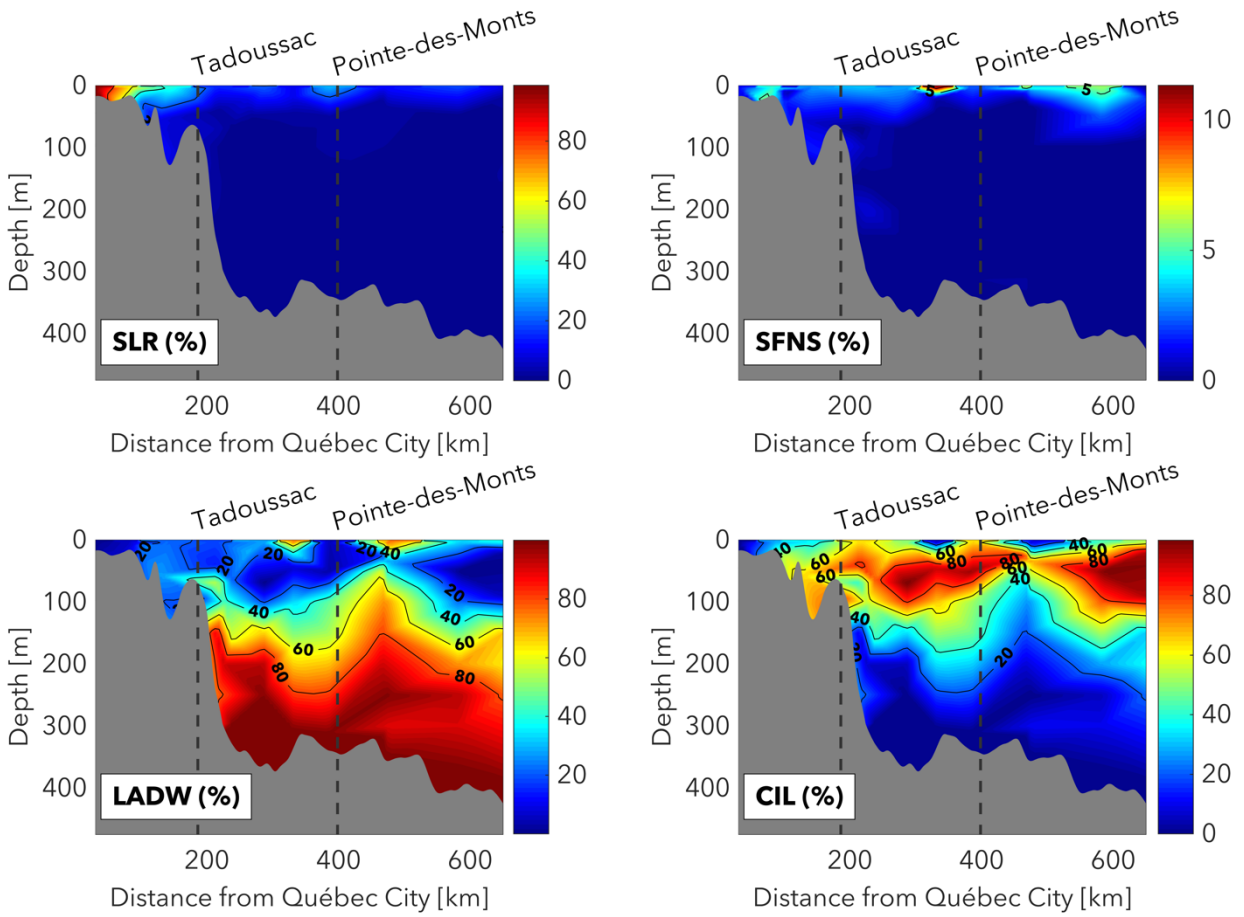

Figure 5. Vertical sections showing the relative contributions (%) of the St. Lawrence River (SLR), Saguenay Fjord and north-shore rivers (SFNS), Labrador/Atlantic deep water (LADW), and Gulf summertime cold intermediate layer (CIL) to the water column structure of the St. Lawrence Estuary and Gulf (May 2016). Linear interpolation was used between the analyzed data points.

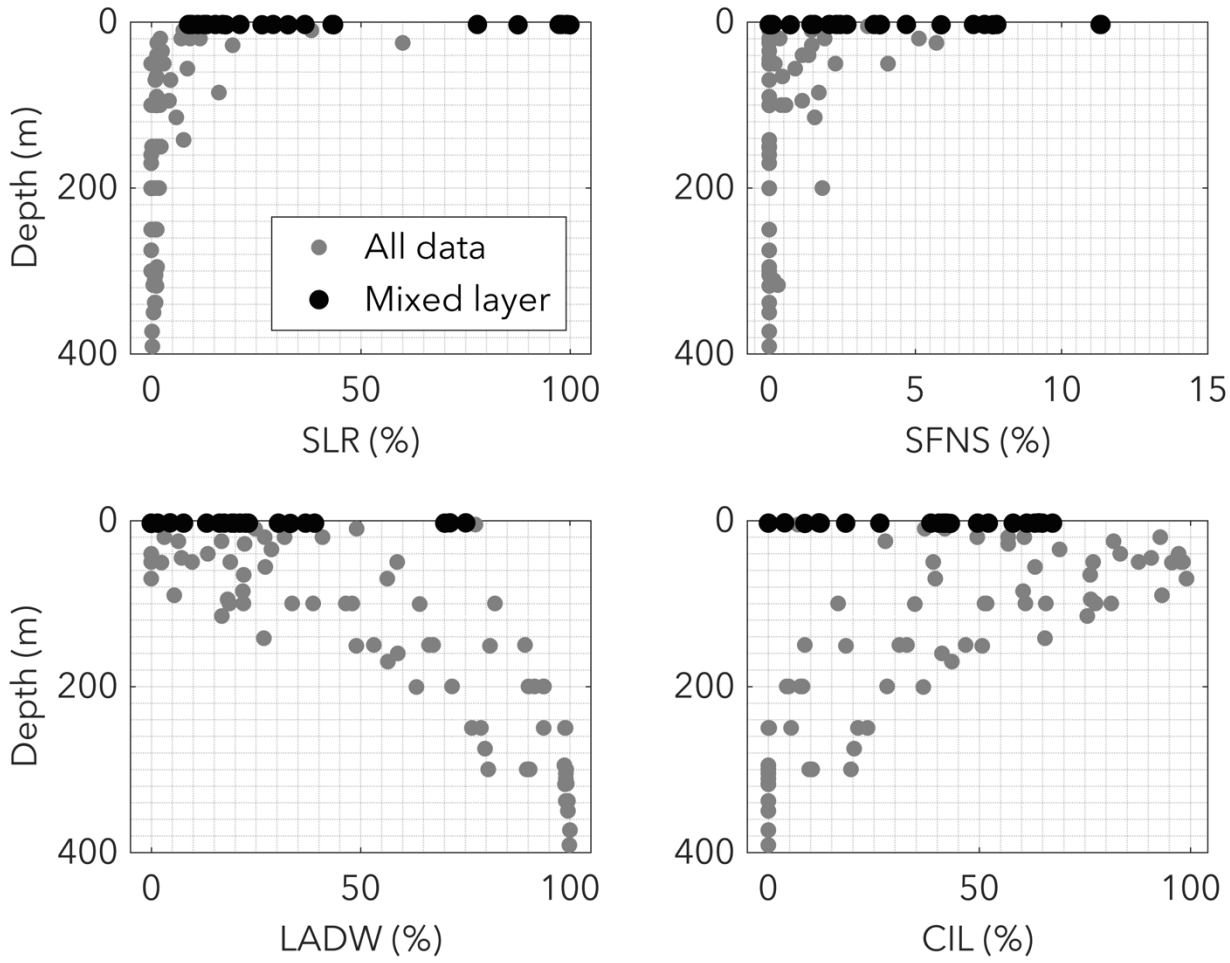

Figure 6. Relative contributions (%) of the St. Lawrence River (SLR), Saguenay Fjord and north-shore rivers (SFNS), Labrador/Atlantic deep water (LADW), and Gulf summertime cold intermediate layer (CIL) as a function of depth. The analyzed data points in the surface mixed layer are highlighted.

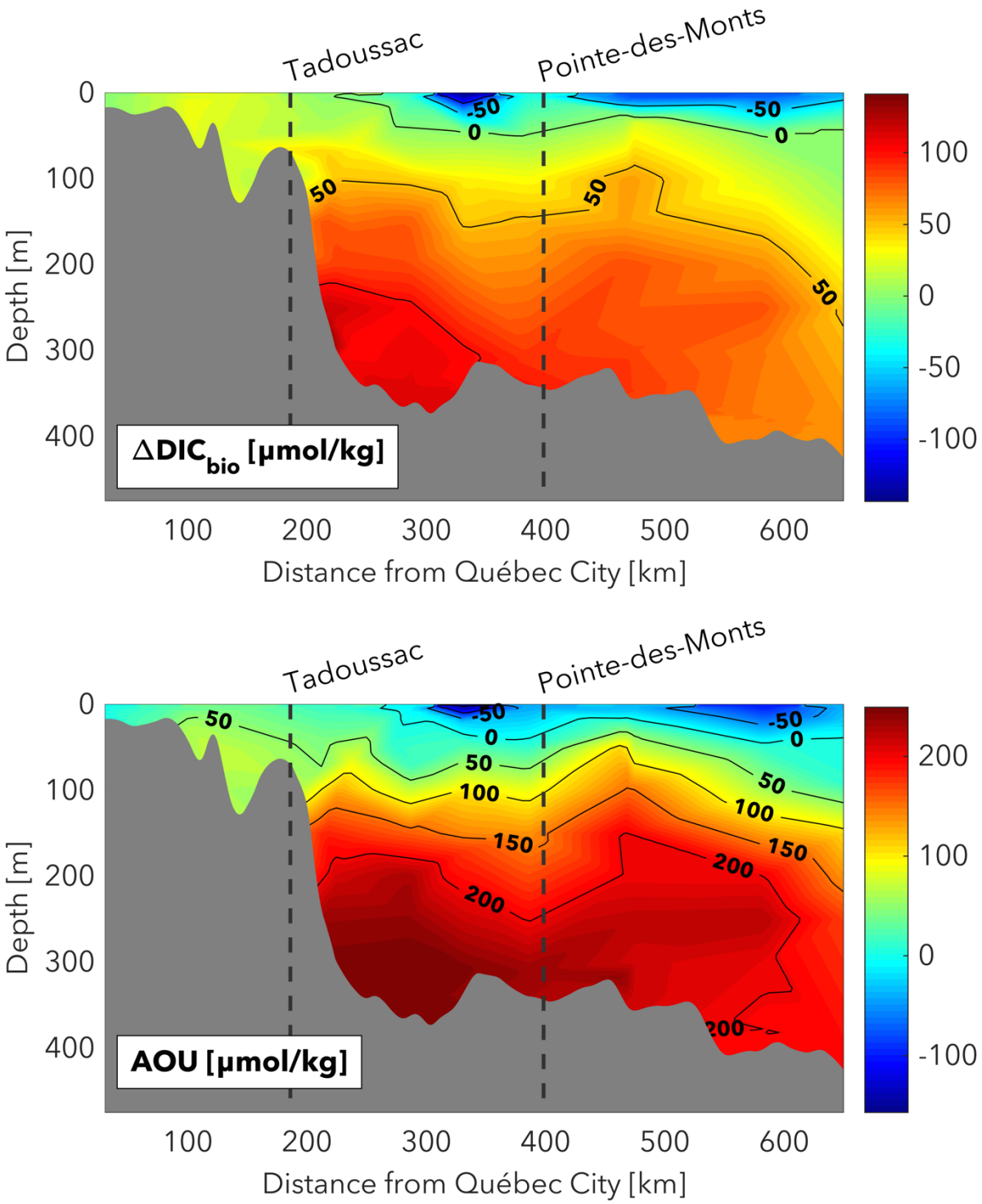

Figure 7. Vertical sections showing ΔDIC_{bio} and AOU. Linear interpolation was used between the analyzed data points.

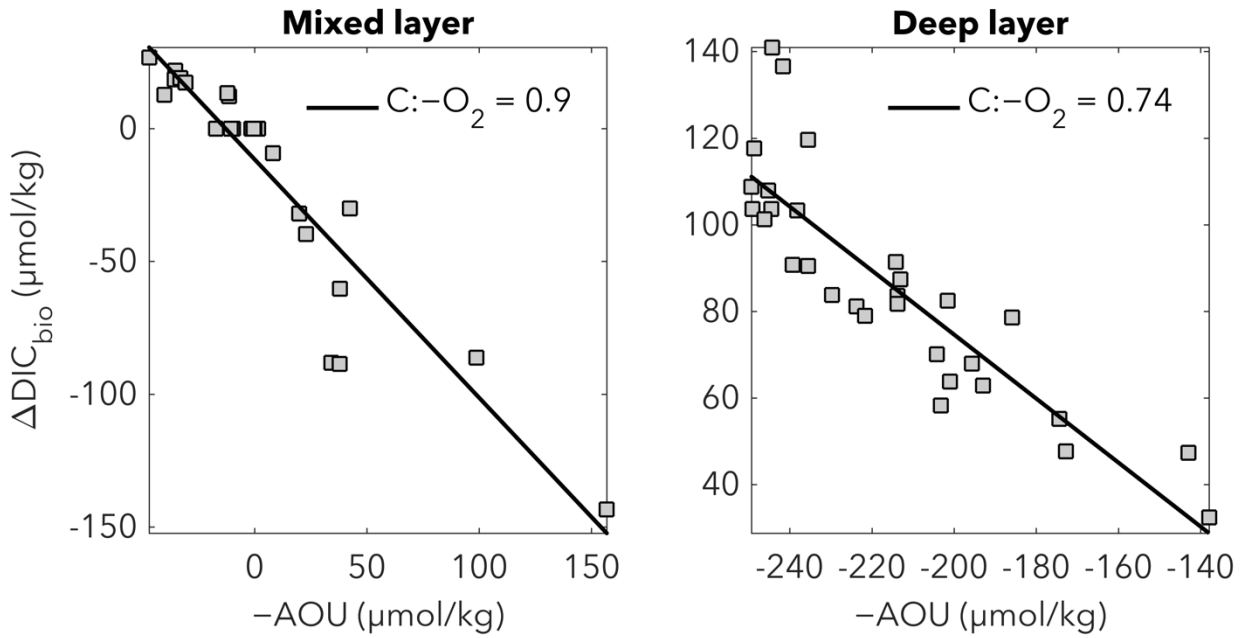

Figure 8. Correlation between ΔDIC_{bio} and AOU in (i) the surface mixed layer and (ii) the deep layer (depth >150 m). For comparison, the $C{:}{-}O_2$ Redfield ratio is ~0.77. AOU has its sign flipped to match the sign convention for ΔO_2.

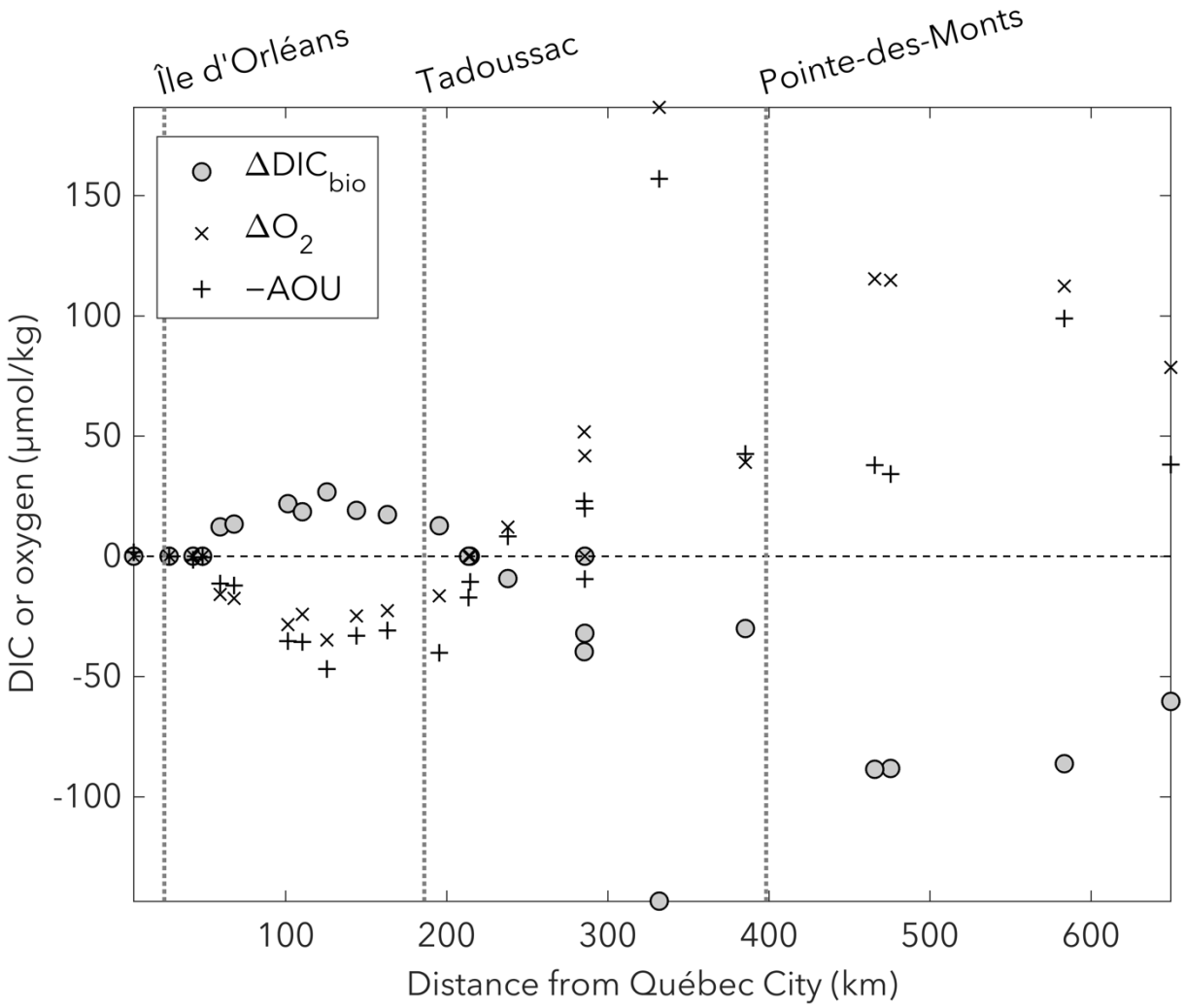

Figure 9. ΔDIC_{bio} in the surface mixed layer as a function of horizontal distance from the head of the Estuary (~5 km downstream of Québec City). ΔO_2 and AOU are included for comparison. AOU has its sign flipped to match the sign convention for ΔO_2.

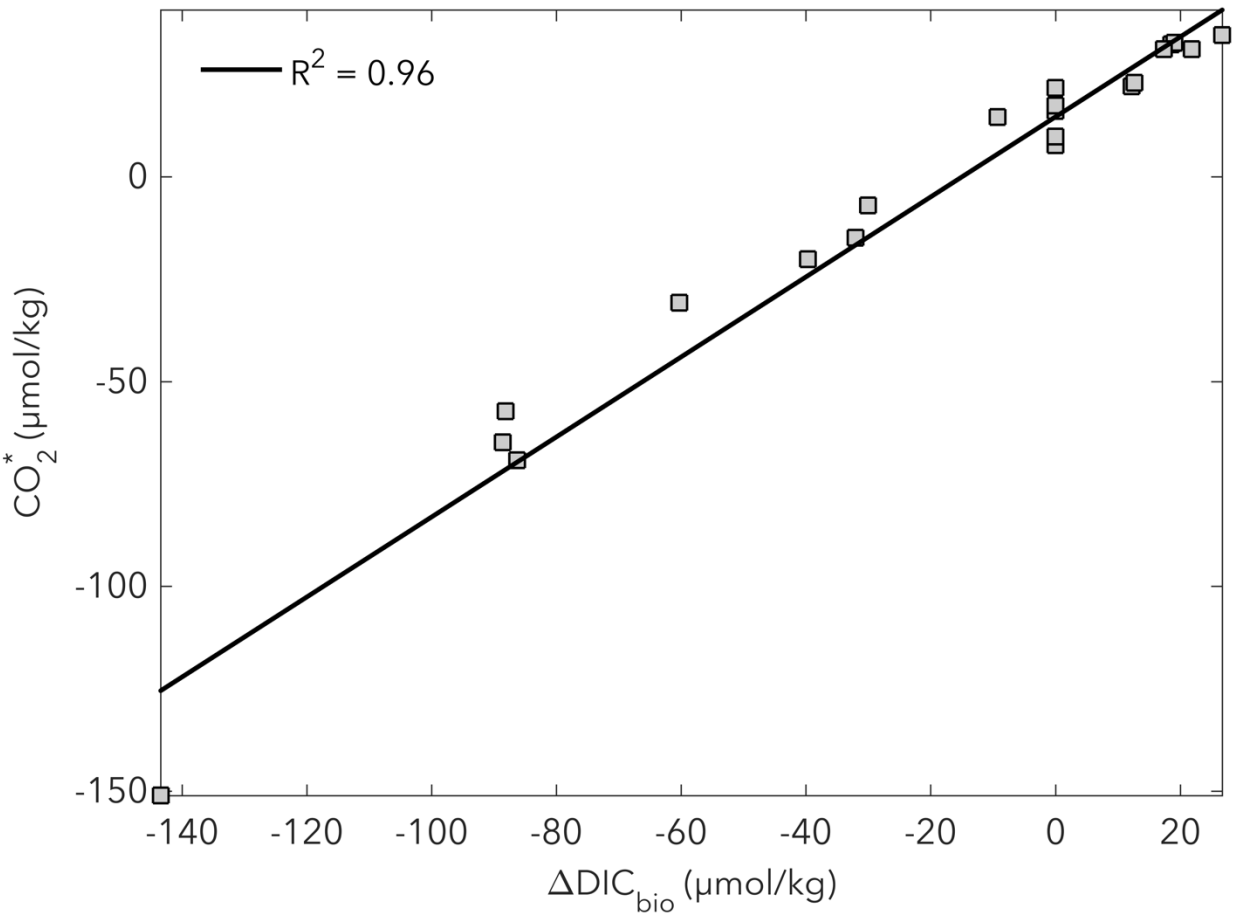

Figure 10. Correlation between CO_2^* (observed DIC concentration minus equilibrium DIC concentration) and ΔDIC_{bio} in the surface mixed layer. As this linear relationship has a slope close to 1 (0.98), it is assumed that excess DIC is mainly influenced by biological activity.

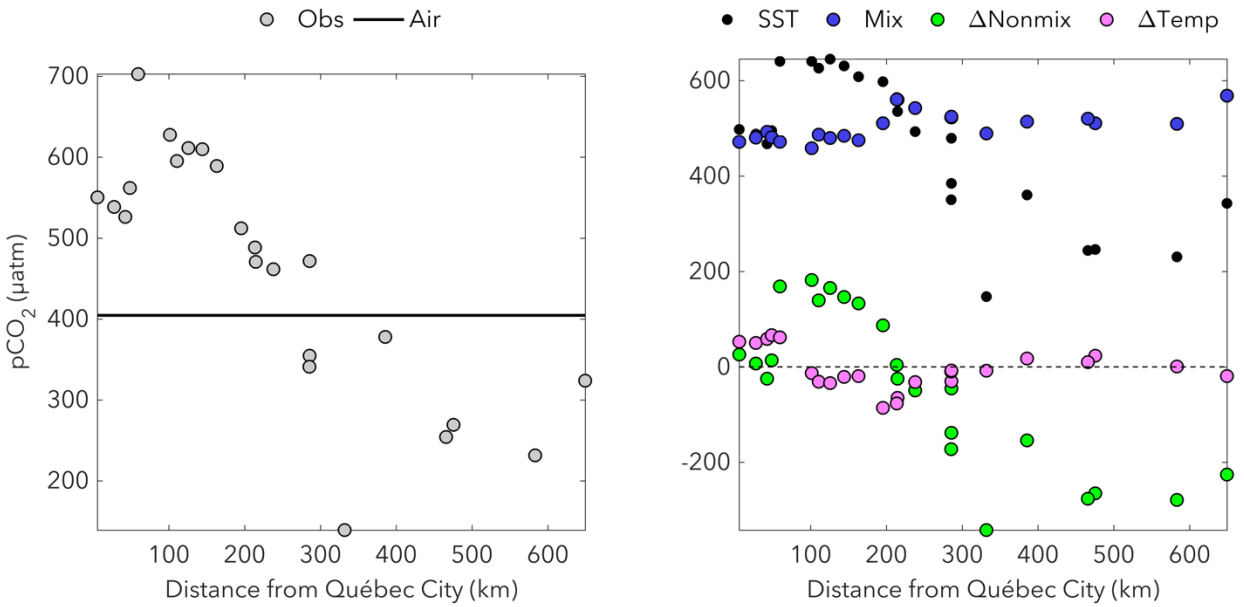

Figure 11. (i) pCO_2(obs) and (ii) $pCO_2(\overline{SST})$, pCO_2(mix), ΔpCO_2(nonmix), and ΔpCO_2(temp) in the surface mixed layer as a function of horizontal distance from the head of the Estuary (~5 km downstream of Québec City). The first term, pCO_2(obs), is the *in situ* pCO_2, whereas the next three terms, i.e., $pCO_2(\overline{SST})$, pCO_2(mix), and ΔpCO_2(nonmix), are normalized to the mean sea surface temperature of the study area in order to remove the effect of temperature on spatial changes in pCO_2 (or ΔpCO_2(temp), equation 1). The horizontal line shows the mean atmospheric pCO_2, pCO_2(air), in May 2016.

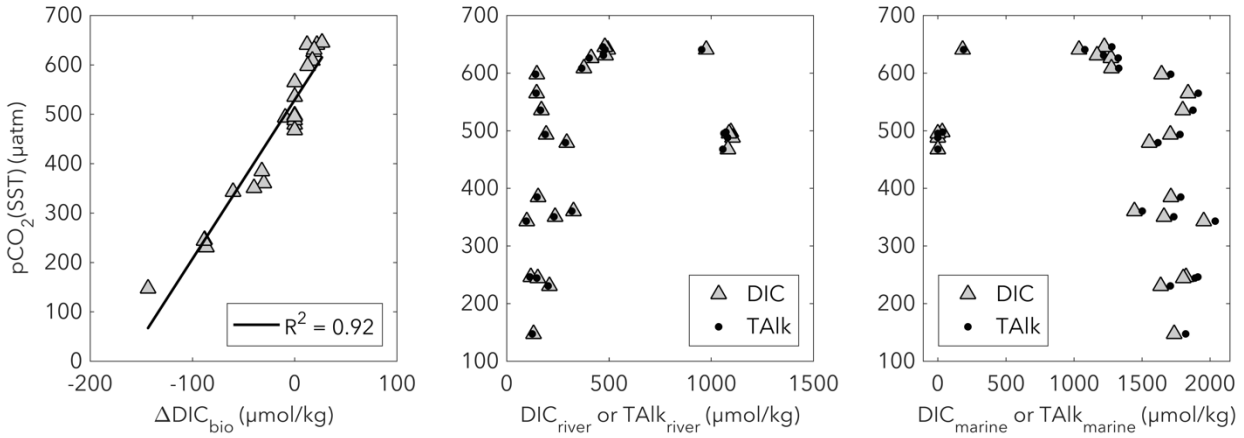

Figure 12. Correlation between $pCO_2(\overline{SST})$ and (i) ΔDIC_{bio} (ii) DIC_{river}, and (iii) DIC_{marine} in the surface mixed layer. $TAlk_{river}$ and $TAlk_{marine}$ are included for comparison.

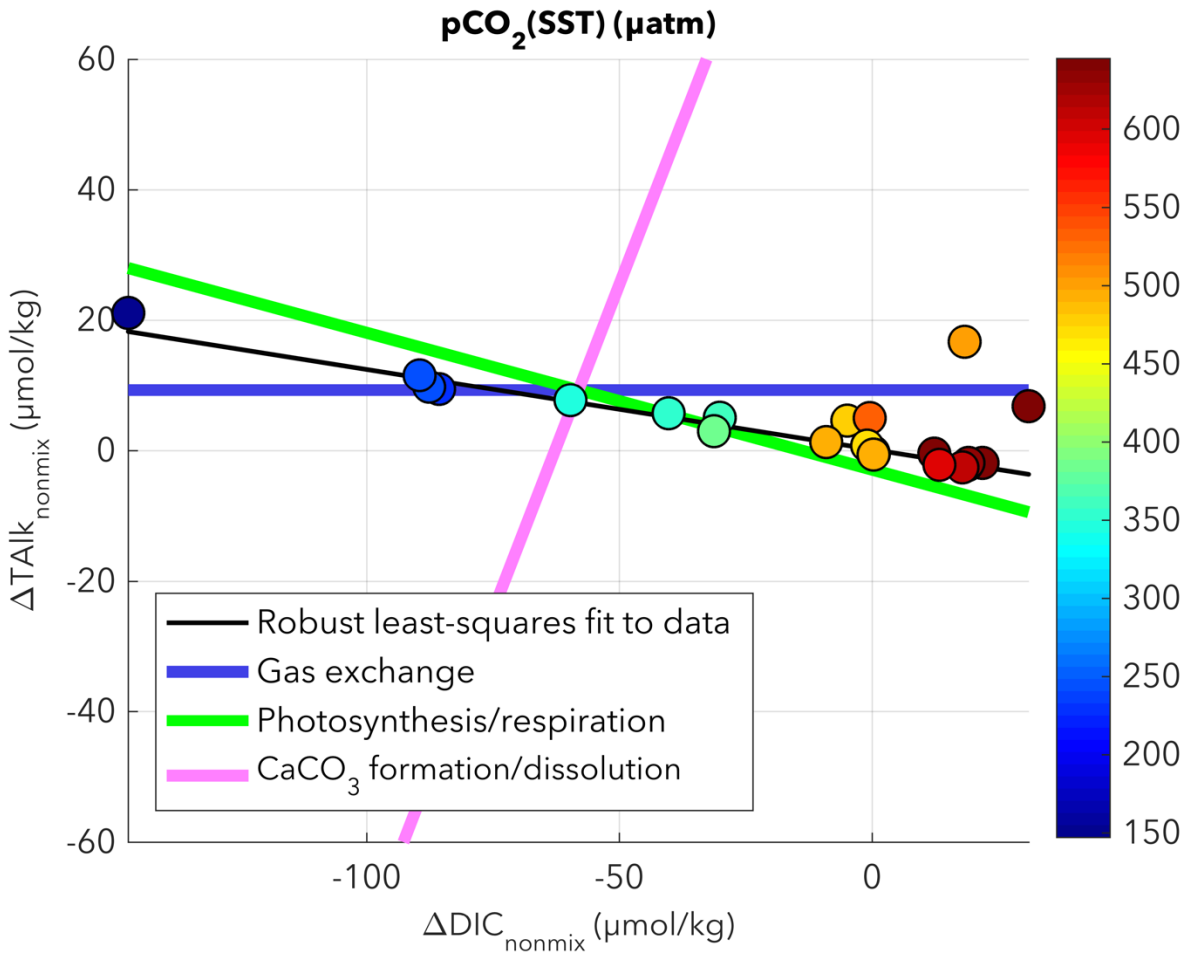

Figure 13. $\Delta TAlk_{nonmix}$ versus ΔDIC_{nonmix} at each observation point in the surface mixed layer. Marker colors show $pCO_2(\overline{SST})$. The solid black line is the least-squares fit to the data using robust regression to minimize the influence of outliers. The heavy lines indicate the major processes controlling the distribution of DIC and TAlk, including air-sea gas exchange (blue), photosynthesis/respiration (green), and calcium carbonate formation/dissolution (pink). The variables ΔDIC_{nonmix} and $\Delta TAlk_{nonmix}$ have been corrected to account for mixing of water masses with different inorganic carbon concentrations. The correction is applied by subtracting DIC_{mix} and $TAlk_{mix}$ from the observed DIC and TAlk, respectively.

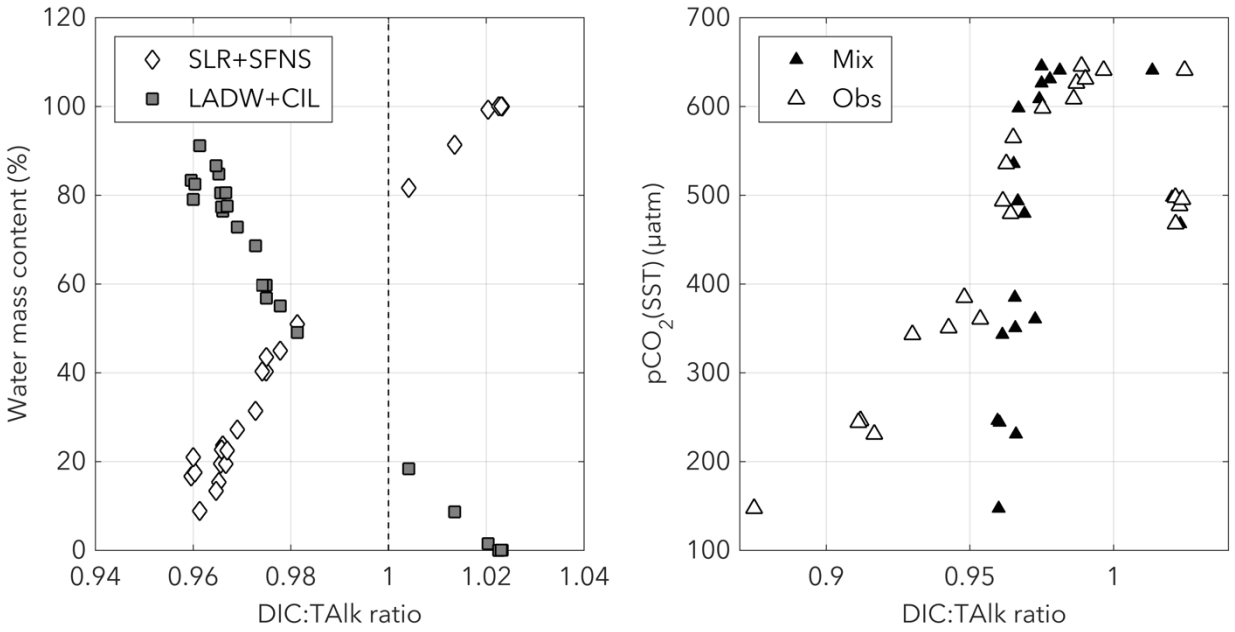

Figure 14. (i) DIC:TAlk ratio in the surface mixed layer as a function of water mass content. The relative contributions of SLR and SFNS were summed to give the percentage of freshwater, whereas the relative contributions of LADW and CIL were summed to give the percentage of seawater. (ii) $pCO_2(\overline{SST})$ versus DIC:TAlk ratio in the surface mixed layer. The filled triangles show the ratio of DIC_{mix} to $TAlk_{mix}$, whereas the open triangles show the ratio of observed DIC to observed TAlk.